RESEARCH ARTICLE

Mitochondrial CISD1/Cisd accumulation blocks mitophagy and genetic or pharmacological inhibition rescues neurodegenerative phenotypes in *Pink1/parkin* models

Aitor Martinez[1,2]*, Alvaro Sanchez-Martinez[1], Jake T. Pickering[1], Madeleine J. Twyning[1], Ana Terriente-Felix[1], Po-Lin Chen[3], Chun-Hong Chen[3] and Alexander J. Whitworth[1]*

Abstract

Background Mitochondrial dysfunction and toxic protein aggregates have been shown to be key features in the pathogenesis of neurodegenerative diseases, such as Parkinson's disease (PD). Functional analysis of genes linked to PD have revealed that the E3 ligase Parkin and the mitochondrial kinase PINK1 are important factors for mitochondrial quality control. PINK1 phosphorylates and activates Parkin, which in turn ubiquitinates mitochondrial proteins priming them and the mitochondrion itself for degradation. However, it is unclear whether dysregulated mitochondrial degradation or the toxic build-up of certain Parkin ubiquitin substrates is the driving pathophysiological mechanism leading to PD. The iron-sulphur cluster containing proteins CISD1 and CISD2 have been identified as major targets of Parkin in various proteomic studies.

Methods We employed in vivo *Drosophila* and human cell culture models to study the role of CISD proteins in cell and tissue viability as well as aged-related neurodegeneration, specifically analysing aspects of mitophagy and autophagy using orthogonal assays.

Results We show that the *Drosophila* homolog Cisd accumulates in *Pink1* and *parkin* mutant flies, as well as during ageing. We observed that build-up of Cisd is particularly toxic in neurons, resulting in mitochondrial defects and Ser65-phospho-Ubiquitin accumulation. Age-related increase of Cisd blocks mitophagy and impairs autophagy flux. Importantly, reduction of Cisd levels upregulates mitophagy in vitro and in vivo, and ameliorates pathological phenotypes in locomotion, lifespan and neurodegeneration in *Pink1/parkin* mutant flies. In addition, we show that pharmacological inhibition of CISD1/2 by rosiglitazone and NL-1 induces mitophagy in human cells and ameliorates the defective phenotypes of *Pink1/parkin* mutants.

*Correspondence:
Aitor Martinez
mtz.aitor@gmail.com
Alexander J. Whitworth
a.whitworth@mrc-mbu.cam.ac.uk
Full list of author information is available at the end of the article

Martinez *et al. Molecular Neurodegeneration* (2024) 19:12

Page 2 of 21

Conclusion Altogether, our studies indicate that Cisd accumulation during ageing and in *Pink1/parkin* mutants is a key driver of pathology by blocking mitophagy, and genetically and pharmacologically inhibiting CISD proteins may offer a potential target for therapeutic intervention.

Keywords CISD1, CISD2, Cisd, Parkinson's disease, Neurodegeneration, Mitophagy, Autophagy, Ageing, PINK1, Parkin, Mitochondria

Graphical Abstract
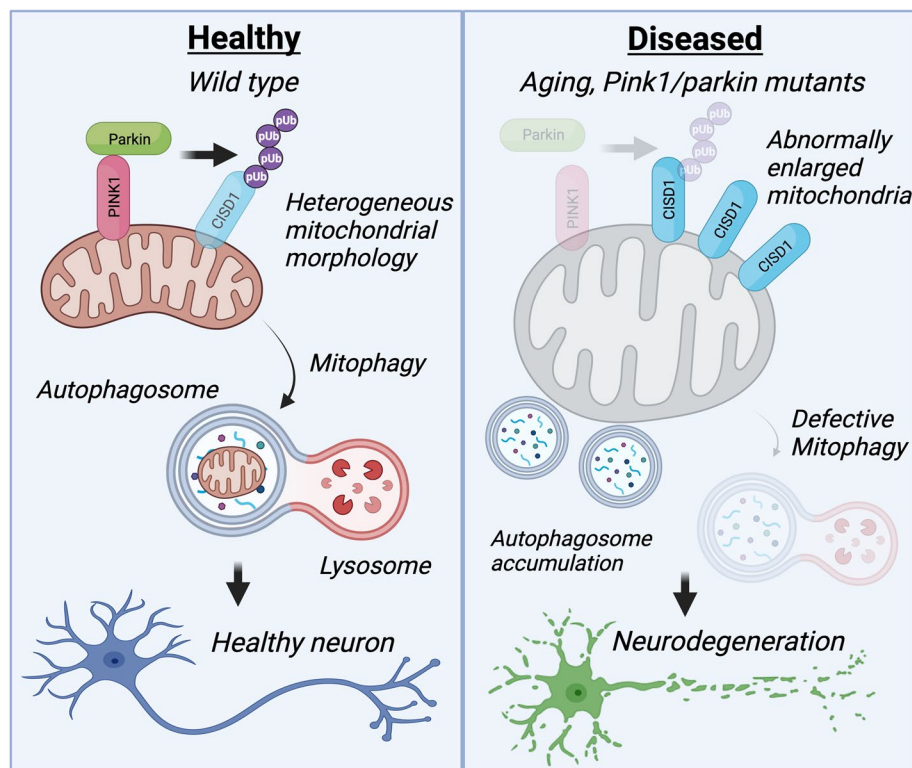
Background

Parkinson's disease (PD) is a common neurodegenerative disorder caused by the progressive loss of midbrain dopaminergic (DA) neurons resulting in a spectrum of clinical symptoms including classic postural instability and loss of motor control as well as many other non-motor symptoms. The cause(s) of selective vulnerability of the neurons lost in PD is not precisely known, with genetic and epidemiological evidence primarily indicating defects in proteostasis, redox balance, calcium handling and mitochondrial homeostasis [1]. Compelling insights have come from understanding the pathogenic mechanisms of inherited forms of PD.

Mutations in the mitochondrial-targeted kinase PINK1 and the E3 ubiquitin ligase Parkin cause familial forms of parkinsonism [2, 3]. A substantial body of evidence supports that PINK1 and Parkin act in a common pathway to promote the degradation of dysfunctional mitochondria through selective autophagy, termed mitophagy. This mechanism involves the stabilisation of PINK1 on the outer mitochondrial membrane (OMM) of dysfunctional mitochondria where it phosphorylates latent ubiquitin bound to OMM-resident proteins. This Ser65-phospho-ubiquitin (pUb) serves as a recruitment signal for Parkin, which is also phosphorylated by PINK1 at Ser65 to activate it, whereupon it additionally ubiquitinates OMM proteins for further phosphorylation triggering proteasomal degradation of specific targets and the recruitment of autophagy receptors, such as p62 [4–6]. In general, mitophagy is considered a key element of mitochondrial quality control (MQC) acting to safeguard a healthy mitochondrial network and prevent age-related

Martinez *et al. Molecular Neurodegeneration* (2024) 19:12

Page 3 of 21

neurodegenerative diseases, such as PD [7]. While many of the molecular details of PINK1/Parkin-mediated mitophagy have been elucidated in cell culture models, in vivo studies have presented a complex picture of the impact of PINK1/Parkin on physiological mitophagy [8–12]. Moreover, the reasons why loss of PINK1 and Parkin activity causes DA neurodegeneration are still not clear, preventing the rational design of targeted therapeutic interventions.

Genetic studies in *Drosophila* have delivered fundamental insights into the biology of the homologous genes, *Pink1* and *parkin* (using FlyBase nomenclature), and the in vivo consequences of their loss. Genetic *Pink1/parkin* null mutants present robust PD-related phenotypes, e.g. locomotor deficits and progressive DA neuron loss, resulting from profound mitochondrial disruption, most notably in flight muscle [3–5]. An unbiased proteomic screen for putative parkin substrates in *Drosophila* neurons highlighted the sole homologue of CISD proteins (here, termed Cisd) as a prevalent ubiquitination target [13]. Indeed, CISD1 and CISD2 have been reported as top Parkin substrates in several human cell culture studies [14–16], cementing these as *bona fide* targets. Moreover, CISD1 has also been found to be a key substrate of the mitochondrial deubiquitinase USP30 [15, 17–19], which has been shown to counteract Parkin function during mitophagy [20]. However, their functional contribution to mitophagy or the downstream phenotypes of *Pink1/parkin* loss have not been studied. Therefore, we sought to study the role of the *Drosophila* Cisd and its human homologues in mitophagy and Pink1/parkin-related neurodegeneration.

CISD proteins (CISD1, CISD2 and CISD3 in vertebrates) belong to the NEET protein family, which are characterised by a unique iron-sulphur [2Fe-2 S] cluster-coordinating CDGSH domain. This positions CISD proteins as important regulators of redox, electron and [2Fe-2 S] cluster transfer reactions, vital for iron metabolism, mitochondrial respiration and the regulation of reactive oxygen species (ROS) production [21]. CISD1/mitoNEET and CISD2/NAF-1 contain a transmembrane domain by which they anchor to OMM and ER, respectively, forming homodimers in each organelle [22]. CISD3/MiNT contains two CDGSH domains acting as a monomer and localises to mitochondrial matrix [23]. CISD1 has been shown to be important for mitochondrial respiration, iron homeostasis and redox balance, as well as a key factor in the export of [2Fe-2 S] clusters from mitochondria [24–27]. CISD2 is a causal gene for Wolfram syndrome, a severe neurodegenerative disease characterised by optic atrophy, deafness, dementia, and juvenile-onset insulin-dependent diabetes mellitus [28]. Furthermore, CISD2 has been shown

to inhibit autophagy and regulate Ca^{2+} release from ER through direct interaction with IP3R, as well as perturbing mitochondrial respiration and cristae structure [29–31].

In this study, we report that *Drosophila* Cisd (also known as Dosmit) accumulates during ageing and in *Pink1/parkin* mutant flies. Cisd overexpression is sufficient to drastically affect mitochondrial morphology, motor behaviour and lifespan, and is particularly toxic when accumulating in neurons. Mechanistically, Cisd accumulation blocks mitophagy and inhibits autophagy flux. Conversely, loss of *Drosophila* Cisd or human CISD1 or 2 is sufficient to promote mitophagy in vivo and in vitro. Consequently, loss of Cisd significantly rescues PD-related phenotypes in *Pink1/parkin* mutants, including motor function and DA neurodegeneration. Finally, we show that the small-molecule CISD inhibitors, rosiglitazone and NL-1, induce mitophagy in cells and are able to partially rescue *Pink1/parkin* fly phenotypes. Thus, pharmacological targeting of CISD proteins represents a new avenue to boost mitophagy and potentially treat PD or other age-related neurodegenerative diseases.

Materials and methods

Drosophila husbandry, stocks and genetics

Drosophila were raised under standard conditions in a temperature-controlled incubator with a 12 h:12 h light:dark cycle at 25 °C and 65% relative humidity, on food consisting of agar, cornmeal, molasses, propionic acid and yeast. Unless specifically indicated otherwise, experiments using adult flies were performed on animals aged ~ 2 days (1–3 d).

Cisd KO ($Cisd^{-/-}$) and *UAS-Cisd* were previously reported [32]. *UAS-ref(2)P* (p62) was generously provided by Prof. D. Walker [33], $park^{25}$ mutants [34], and *UAS-mito-QC* [8] lines have been previously described. $Pink1^{B9}$ mutants [35] were kindly provided by Prof. J. Chung (Seoul National University). The following strains were obtained from Bloomington *Drosophila* Stock Center (BDSC, RRID:SCR_006457): w^{1118} (BDSC_6326), *da-GAL4* (BDSC_55850), *nSyb-GAL4 (*BDSC_51635), *Mef2*-GAL4 (BDSC_27390), *TH*-GAL4 (BDSC_8848), *UAS-lacZ* (BDSC_8529), *UAS-mito-GFP* (BDSC_8843), *UAS-hCISD1* (BDSC_77990), *UAS-hCISD2* (BDSC_76845), *UAS-Atg5 RNAi* (BDSC_27551), *UAS-Atg8a* (BDSC_84981), *UAS-GFP-mCherry-Atg8a* (BDSC_37749) and *UAS-mCherry-Atg8a* (BDSC_37750, [36]). The following strains were obtained from Vienna Drosophila Research Centre (VDRC): *UAS-lacZ RNAi* GD (v51446), *Cisd RNAi* GD (v33925) and KK (v104501).

Where multiple UAS transgenes were present in experimental animals, an inert UAS transgene (e.g., UAS-*lacZ*, UAS-*lacZ RNAi*, UAS-*fluorophore*, etc.), appropriate

Martinez *et al. Molecular Neurodegeneration* (2024) 19:12

Page 4 of 21

for the experimental conditions, was always included to account for possible titration effects. Since X chromosome nondisjunction is present in multiple balanced *Pink1*[B9] mutant stocks, correct genotypes were determined by either combining paternal animals with X chromosome markers or by PCR-based genotyping of discarded tissue after dissection.

Antibodies and reagents

The following mouse antibodies were used: ATP5A (Abcam, ab14748, 1:10000), Ubiquitin (clone P4D1, Cell Signalling Technology, 3936, 1:1000), CISD2 (Proteintech, 66082-1-Ig, 1:1000), TOM20 (clone F-10, Santa Cruz, sc-17,764, 1:1000), HA (Cell Signaling, 2367, 1:1000), tyrosine hydroxylase (Immunostar, 22,491), Tubulin (Sigma, T9026, 1:5000). The following rabbit antibodies were used in this study: pS65-Ub (Cell Signaling Technologies, 62,802 S, 1:1000), GABARAP/Atg8a (Abcam, ab109364, 1:1000), ref(2)P/p62 (Abcam, ab178440, 1:1000), PINK1 (Cell Signaling Technology, 6946, 1:1000), CISD1 (Proteintech, 16006-1-AP, 1:1000), CISD2 (Proteintech, 13318-1-AP, 1:1000), FLAG (Cell Signaling, 2368 S, 1:1000), Tubulin (Abcam, ab18251, 1:5000). Rat anti-Calnexin (clone W17077C, BioLegend, 699,401).

The following secondary antibodies were used: Goat anti-mouse-HRP (Abcam, Ab6789-1, 1:10000), Goat anti-rabbit-HRP (Invitrogen, G21234, 1:10000), Goat anti-mouse-IRDye 680RD (Li-Cor, 926-68070), Goat anti-rabbit- IRDye 800CW (Li-Cor, 926-32211), Goat anti-mouse-AF405 (Invitrogen, A48255), Goat anti-mouse-AF488 (Invitrogen, A11001), Goat anti-mouse-AF594 (Invitrogen, A11005), Goat anti-rabbit-AF488 (Invitrogen, A11008) and Donkey anti-rat-AF488 (Invitrogen, A21208).

DMEM/F12, GlutaMAX Supplement (31,331,093, Gibco), DMEM, high glucose, GlutaMAX Supplement, pyruvate (31,966,047, Gibco), Fetal Bovine Serum (FBS) (10,270,106, Gibco), MEM Non-Essential Amino Acids Solution (100X) (11,140,050, Gibco), Penicillin-Streptomycin (10,000 U/mL) (15,140,122, Gibco), Opti-MEM (31,985,062, Gibco), Lipofectamine RNAiMAX (13,778,075, Invitrogen), Lipofectamine3000 (L3000008, Invitrogen), phosphate buffered saline (DPBS (1X), no calcium, no magnesium, 14190-169, Gibco), Formaldehyde (FA) (28,908, Fisher Scientific Ltd) and Pierce BCA Protein Assay Kit-500 mL (23,223, Life Technologies) were purchased from Thermo Fisher Scientific. The following reagents were obtained from Sigma: Dimethyl sulfoxide (DMSO) (276855-250ML), Rosiglitazone (R2408-50MG), Antimycin A (A8674-25MG). 5X siRNA Buffer (B-002000-UB-100, Horizon Discovery), mitoNEET Inhibitor NL-1 (475825-10MG, Calbiochem),

cOmplete protease inhibitors (4,693,159,001, Roche), PhosSTOP phosphatase inhibitors (4,906,837,001, Roche), Bovine Serum Albumin (BSA, Fraction V, Cold-ethanol Precipitated, BP1605100, Fisher BioReagents), Oligomycin A (495455-10MG, Merck Life Science Limited), Chloroquine (C6628-25G, Merck Life Science Limited).

Cell culture, transfection, RNA interference and drug treatment

ARPE-19 cells, stably expressing mCherry-GFP-Fis1(101–152) referred to as ARPE-19-MQC, were a kind gift of Dr Ian Ganley (University of Dundee), and hTERT-RPE1, hTERT-RPE1-YFP-PARKIN cells were generously donated by Prof. Jon D Lane (University of Bristol). Cells were cultured in Dulbecco's modified Eagle's medium DMEM/F12 (hTERT-RPE1, hTERT-RPE1-YFP-PARKIN, and ARPE-19-MQC) or DMEM (U2OS) supplemented with 10% FBS, 1% non-essential amino acids and 1% penicillin/streptomycin. For siRNA experiments, cells were reverse-transfected with 20 nM of non-targeting (NT1) or target-specific siRNA oligonucleotides (Dharmacon On-Target Plus or siGenome, ThermoFisher Scientific), using Lipofectamine RNAi-MAX (Invitrogen) according to manufacturer's instructions for 72 h. Alternatively, cells were seeded and transfected for 48 h with pcDNA3.1-CISD1-FLAG or pcDNA3.1-CISD2-FLAG using Lipofectamine3000 (Invitrogen) as per manufacturer instructions. For drugs treatment experiments, cells were treated with 100 µM of rosiglitazone or NL-1 for 24 h.

siRNA and plasmids

siRNAs used in this manuscript were as follows: ON-TARGETplus Non-Targeting siRNA oligo #1 (D-001810-01-20, Horizon Discovery), ON-TARGETplus Human CISD1 siRNA SMARTpool (L-020954-01-0020, Horizon Discovery), ON-TARGETplus Human CISD2 siRNA SMARTpool (L-032593-02-0020, Horizon Discovery). ORFs from hCISD1 and hCISD2 were amplified from transgenic flies carrying hCISD1 (BDSC_77990) or hCISD2 (BDSC_76845). FLAG was introduced at the C-terminal during the PCR amplification. Gibson assembly was used to introduce these PCR products into a pcDNA3.1 cut with KpnI and NotI. The following primers were used for the PCR amplification:

hCISD1_KpnI_pcDNA31_Fwd: CTGGCTAGCGTTTAAACTTAAGCTTGGTACCATGAGTCTGACTTCCAGTTCCA.
hCISD1_FLAG_NotI_Rev: AAACGGGCCCTCTAGACTCGAGCGGCCGCCTACTTGTCATCGTCG

Martinez *et al. Molecular Neurodegeneration* (2024) 19:12

Page 5 of 21

TCCTTGTAGTCAGTTTCTTTTTTCTTGATG
ATCAGAG.
hCISD2_KpnI_pCDNA31_Fwd: CTGGCTAGC
GTTTAAACTTAAGCTTGGTACCATGGTGCT
GGAGAGCGTGG.
hCISD2_FLAG_NotI_Rev: AAACGGGCCCTCTAG
ACTCGAGCGGCCGCCTACTTGTCATCGTCG
TCCTTGTAGTCTACTTCTTTCTTCTTCAGT
ATTAGTG.

Drosophila and cell cultures harvesting and lysis

For the analysis of cell culture lysates by immunoblot, cells were rinsed once with cold PBS and subsequently lysed with 100–200 µL cold RIPA buffer (50 mM Tris pH8, 180 mM NaCl, 1mM EDTA, 1% Triton-X100, 0.5% SDS), supplemented with cOmplete protease inhibitors and phosphatase inhibitors. Cell lysates were incubated on ice for 15-20 min before being harvested into an Eppendorf tube. In the case of *Drosophila* lysates, animals (5 to 20 per replicate) with the right genotype were selected under CO_2 and flash-frozen in liquid N_2, all direct comparing genotypes being harvested equally at the same time. 150–200 µL of ice-cold RIPA buffer supplemented with cOmplete protease inhibitors and phosphatase inhibitors was added to 2 mL tubes containing 1.4 mm ceramic beads (15,555,799, Fisherbrand) to which flies were added and lysed using a Minilys homogeniser (Bertin Instruments). Flies were shaken twice at maximum speed, 10 s followed by a brief incubation on ice, after which samples were shaken again at maximum speed, 10 s, making a total of three cycles. After the lysis, *Drosophila* samples were returned to ice for at least 40 min. Both cell culture and *Drosophila* lysates were then centrifuged 5 min at maximum speed (21,000 x g) at 4 °C. Supernatant was then transferred to a fresh Eppendorf tube and centrifuged. This step was repeated until samples were completely cleared. For experiments evaluating Cisd dimer bands (reducing vs. non-reducing conditions), RIPA buffer was additionally supplemented with fresh 20 mM iodoacetamide.

Immunoblotting

Protein content was determined by BCA assay as per manufacturer instructions. Samples were then diluted in Laemmli ×4 Sample Buffer (1,610,747, Bio-Rad) supplemented with 100 mM 2-Mercaptoethanol and analysed by SDS-PAGE using Mini-PROTEAN TGX Gels 4–20% (4,561,093, Bio-Rad) or similar. Gels were transferred onto precast nitrocellulose membranes (1,704,158, Bio-Rad) using the BioRad Transblot Turbo transfer system, and membranes were immediately washed in distilled water and stained with ponceau (P7170-1 L, Sigma)

Membranes were then blocked by incubation with 5% (w/v) semi-skimmed milk in TBS 1X containing 0.1% (v/v) Tween-20 (TBStw) for 1 h at least. Membranes were then incubated in a shaker at 4 °C overnight with appropriate primary antibodies in 5% milk-TBStw. 3 washes of 10 min with TBStw were performed to rinse the membranes and then were incubated for one hour in secondary antibodies made in 5% milk-TBStw. Membranes were then washed 3 times,10 min each, in TBStw. Membranes were developed either with ECL reagent (RPN2232, Amersham) using the Amersham Imager 680 (GE Healthcare), or alternatively with the LICOR secondary antibodies and imaged in an Odyssey LICOR imaging system. Image analysis was performed using of FIJI (Image J). For experiments evaluating Cisd dimer bands (reducing vs. non-reducing conditions), samples were diluted either in Laemmli x4 Sample Buffer supplemented with 100 mM 2-Mercaptoethanol (reducing) and/or in Laemmli x4 Sample Buffer alone (non-reducing conditions).

Quantitative real-time PCR (qRT-PCR)

5 adult flies per biological replicate were homogenised in TRIzol and RNA extraction was carried out using Directzol RNA MiniPrep kit (Zymo Research, Z2050). DNA was removed with Turbo DNase free (Ambion, AM1907), and cDNA synthesis was performed using a Maxima First Strand kit (ThermoFisher, K1641) followed by a qRT-PCR using SYBR green (ThermoFisher, 4,309,155) with a CFX96 Touch Real-Time PCR Detection System. The relative transcript levels of each target gene were normalised against *RpL32* and *Tubulin* (*Tub84B*) mRNA levels; quantification was performed using the comparative C_T method [37]. Primers used:

Tubulin - Fwd: TGGGCCCGTCTGGACCACAA; Rev: TCGCCGTCACCGGAGTCCAT [38],
RPL32 - Fwd: GCCGCTTCAAGGGACAGTATCTG; Rev: AAACGCGGTTCTGCATGAG [39],
Pink1 - Fwd: AACAGTCCGGAGATCCTACAG; Rev: GACGACCCTCGCACATAA [40], and.
Parkin - Fwd: AGTACACCGTGGACCCAAAT; Rev: TGTGCTGACTTTGATGGTGA [40].

Immunohistochemistry and sample preparation of *Drosophila*

Drosophila brains were dissected from 30-day-old flies and immunostained with anti-tyrosine hydroxylase as described previously [41]. Tyrosine hydroxylase-positive neurons were counted under blinded conditions. For immunostaining of adult flight muscles and larval brains, animals were dissected in PBS 1X and fixed in 4% FA/

PBS for 30 min at room temperature, permeabilized in 0.3% Triton X-100 for 30 min, and blocked with 1% BSA in 0.3% Triton X-100 PBS for 1 h at RT. Tissues were then incubated on a shaker with the appropriate primary antibody: ATP5A antibody (Abcam, ab14748, 1:500), pUb (pS65-Ub, Cell Signalling Technologies, 62,802 S, 1:250) and/or ref(2)P/p62 (Abcam, ab178440, 1:1000), diluted in 1% BSA in 0.3% Triton X-100 PBS overnight at 4 °C. Next day, samples were rinsed 3 times 10 min with 0.3% Triton X-100 in PBS, and incubated with the appropriate fluorescent secondary antibodies overnight at 4 °C. The tissues were washed 3 times in 0.3% Triton X-100 in PBS followed by a last wash on PBS and mounted on slides using Prolong Diamond Antifade mounting medium (Thermo Fisher Scientific) and imaged next day. Tissues were imaged with a Zeiss LSM880 confocal microscope (Carl Zeiss MicroImaging) equipped with a Nikon Plan-Apochromat 63x/1.4 NA oil immersion objective. Images were analyses using FIJI (Image J).

Mitochondrial morphology in larval brains
Third instar larvae overexpressing *UAS-mito-GFP* with the pan-neuronal driver *nSyb-GAL4* were dissected in PBS and fixed in 4% FA/PBS for 30 min at room temperature. The tissues were washed 3 times in PBS and mounted on slides using Prolong Diamond Antifade mounting medium (Thermo Fisher Scientific) and image next day in a Zeiss LSM880 confocal microscope (Carl Zeiss MicroImaging) equipped with Nikon Plan-Apochromat 63x/1.4 NA oil immersion objectives.

Locomotor and lifespan assays
The repetitive iteration startle-induced negative geotaxis (RISING, or 'climbing') assay was performed using a counter-current apparatus. Experiments were performed using multiple small groups of flies of the indicated genotypes and ages. Briefly, flies were collected under minimal CO_2 anaesthesia 24 h before the assay. On the day of assay, flies are transferred to assay tubes and allowed to acclimatise in the behaviour room for ~ 1 h. Cohorts of ~ 20 flies (25 max.) were placed into the first chamber of the counter-current apparatus, tapped to the bottom and given 10 s to climb a 10 cm distance. Flies that climbed > 10 cm within this time were shifted to the neighbouring tube. This procedure was repeated five times, and the number of flies that remained in each chamber were counted. The weighted performance of several groups of flies for each genotype was normalised to the maximum possible score and expressed as the *climbing index* [34]. To age flies for climbing assays, they were transferred to fresh tubes every 2–3 days. For lifespan experiments, flies were grown under identical conditions at low density. Progeny were collected under very light (< 30 s) anaesthesia and kept in tubes of 10–25, transferred to fresh media every 2–3 days and the number of dead flies recorded. Percent survival was calculated at the end of the experiment after correcting for any accidental loss or escape using https://flies.shinyapps.io/Rflies/ (Luis Garcia).

Image analysis and quantification of mitolysosomes in *Drosophila* tissues
For mitolysosome imaging in *UAS-mito-QC*, tissues were dissected in PBS, fixed in 4% FA/PBS at pH 7 for 30 min at room temperature and mounted. Third instar larval and adult brains were mounted in Prolong Diamond Antifade mounting medium (Thermo Fisher Scientific), while thoraces were mounted in VECTASHIELD Antifade Mounting Medium (H-1000, Vector Laboratories). Larval and adult brains were imaged using Andor Dragonfly spinning disk microscope (Oxford Instruments Group), equipped with a Nikon Plan-Apochromat 100x/1.45 NA oil immersion objective and iXon camera taking 10–13 µm z-stacks with 0.2 µm step size. Adult thoraces were imaged with a Zeiss LSM 880 confocal microscope (Carl Zeiss MicroImaging) equipped with Nikon Plan-Apochromat 63x/1.4 NA oil immersion objectives, taking 10 µm z-stacks with 1 µm step size. We find that the time elapsed from dissection-mounting and imaging is critical for the retrieval of red-only dots. Tissue specific optimisation was required. Larval brains were imaged early next day after dissection, while adult brains and thoraces were imaged briefly after (2–4 h later). Image analysis of larval brains was done employing Imaris (version 9.7.0) analysis software (BitPlane; RRID:SCR_007370) as previously described [8]. For adult *Drosophila* brains and thoraces, as well as for ARPE-19-MQC cells, mitolysosomes were analysed using the FIJI plug-in *mito-QC Counter* [42] as advised by authors. Analysis was performed in maximum projection images of *Drosophila* adult brain and ARPE-19-MQC cells, while *Drosophila* adult thoraces were analysed as per single plane.

The average number of mitolysosomes per cell was analysed per animal in larval and adult brain, as well as in ARPE-19-MQC cells, while mitolysosomes per area (µm) was calculated in *Drosophila* muscles. Data points in the quantification charts show the average mitolysosomes per biological replicate, where $n \geq 6$ animals or $n \geq 60$ cells for each condition.

Transmission electron microscopy
Thoraces were dissected in 0.1 M cacodylate buffer and fixed in 1% glutaraldehyde and 4% paraformaldehyde in 0.1 M cacodylate buffer overnight at 4 °C. After washing with 0.1 M cacodylate buffer, the samples were treated with 1% OsO_4 for 1 h at 4 °C. After washing with ddH_2O,

Martinez *et al. Molecular Neurodegeneration* (2024) 19:12

Page 7 of 21

the samples were dehydrated in a gradient series using 30%, 50%, 70%, 95%, and 100% ethanol solutions at room temperature. The samples were then infiltrated using series epoxy resin at room temperature and mounted in pure resin. After polymerization at 60 °C for 2 days, 90 nm sections were prepared and observed with a Tecnai G2 Spirit TWIN transmission electron microscope (FEI, Hillsboro, OR, USA).

Imaging and analysis of autolysosomes using GFP-mCherry-Atg8a reporter in *Drosophila*

Adult muscle from GFP-mCherry-Atg8a reporter *Drosophila* were dissected in PBS, fixed with 4% FA/PBS at pH 7 for 30 min at room temperature, and mounted in Prolong Diamond Antifade mounting medium (Thermo Fisher Scientific). Samples were imaged the day after. Confocal images, acquired with a Zeiss LSM 880 microscope (Carl Zeiss MicroImaging) equipped with Nikon Plan-Apochromat 63x/1.4 NA oil immersion objectives, taking 10 µm z-stacks with 1 µm step size, were processed using FIJI plug-in *mito-QC Counter* [42]. The quantification of autolysosomes was performed in a plane-by-plane basis similarly to mitolysosome analysis in muscles. Data points in the quantification charts show average autolysosomes per area (µm) for individual animals, where $n \geq 6$ animals for each condition.

ARPE-19-mito-QC cell based mitophagy analysis

ARPE-19-mito-QC-FIS1 (Ian Ganley, University of Dundee) cells were used to assess mitophagy in a human cell model. After 48 h knockdown with siRNA oligos, cells were seeded onto an Ibidi dish (IB-81,156, Ibidi, Thistle Scientific Ltd), and at 72 h post-knock down cells were imaged live using a spinning disk microscope. Generated images were processed using the FIJI plug-in *mito-QC Counter* [42] as previously described. For treatments with rosiglitazone and NL-1: cells were seeded onto an Ibidi dish, next day were treated with 100 µL rosiglitazone or NL-1 for 24 h and imaged and analysed as described above.

Mitochondrial enrichment by differential centrifugation

All steps were performed on ice or at 4 °C. 20–30 flies were prepared either fresh or after flash-freezing in liquid nitrogen, with all direct comparisons performed with flies that were prepared in the same manner. Flies were transferred into a Dounce homogeniser containing 400 µL of mitochondrial isolation buffer (225 mM mannitol, 75 mM sucrose, 5 mM HEPES, 0.1 mM EGTA, pH 7.4) containing cOmplete protease inhibitors (Roche) and PhosSTOP phosphatase inhibitors (Roche), and manually homogenised with 15 strokes of a pestle. The homogenate was transferred to an Eppendorf tube, after which further

400 µL of mitochondrial isolation buffer was added to the homogeniser and the sample was homogenised with a further 5 strokes. The homogenates were pooled and centrifuged at 1500 g at 4 °C for 6 min before being filtered through a 70 µm nylon cell strainer (352,350, Falcon). The sample was then centrifuged at 7000 g at 4 °C for 6 min and the resulting mitochondrial pellet was washed with isolation buffer once and finally resuspended into 150–200 µL RIPA buffer. The protein content was determined by BCA assay (Thermo Pierce).

USP2 deubiquitination assay

For the assessment of ubiquitinated Cisd in mitochondrial fractions, USP2 deubiquitinating assay was performed as previously described [43]. 30 µg protein per mitochondrial fraction was treated with the pan-specific deubiquitinase USP2 (E-506, BostonBiochem). The USP2 enzyme was diluted in buffer (50 mM Tris–pH 7.5, 50 mM NaCl, 10 mM DTT) and then added to the subcellular fractions to a final USP2 concentration of 1 µM. The mixture was incubated for 45 min at 37 °C prior to analysis by immunoblotting.

Rosiglitazone treatment in *Drosophila*

Parental crosses were set on food containing 1 mM rosiglitazone diluted 1:1000 or DMSO as control. Resultant progeny of 0–3 days old were anaesthetised with CO_2 and the correct genotype was selected for further investigation.

Light microscopy imaging of *Drosophila* thorax indentations and wing posture

0–3 days old flies were anaesthetised with CO_2 and thorax indentations and abnormally extended wing posture were assessed by light microscopy imaging using a Nikon SMZ stereo zoom microscope fitted with 1x Apo lens. The number of animals displaying each phenotype was counted in a binary manner (present-absent) respective to the total.

Data presentation and statistical analysis

Charts report data as mean ± 95% CI for climbing behaviour or mean ± SEM for all other data sets. The number of biological replicates (N) are shown in individual graphs as individual data points or numerical value when $N > 15$. For statistical analyses of lifespan experiments, a log rank (Mantel-Cox) test was used. For climbing assay and qRT-PCR analyses, a Kruskal-Wallis nonparametric test with Dunn's post-hoc correction for multiple comparisons was used. Where multiple groups were compared, statistical significance was calculated by one-way ANOVA with Bonferroni, Sidak's or Geisser-Greenhouse post-test correction for multiple
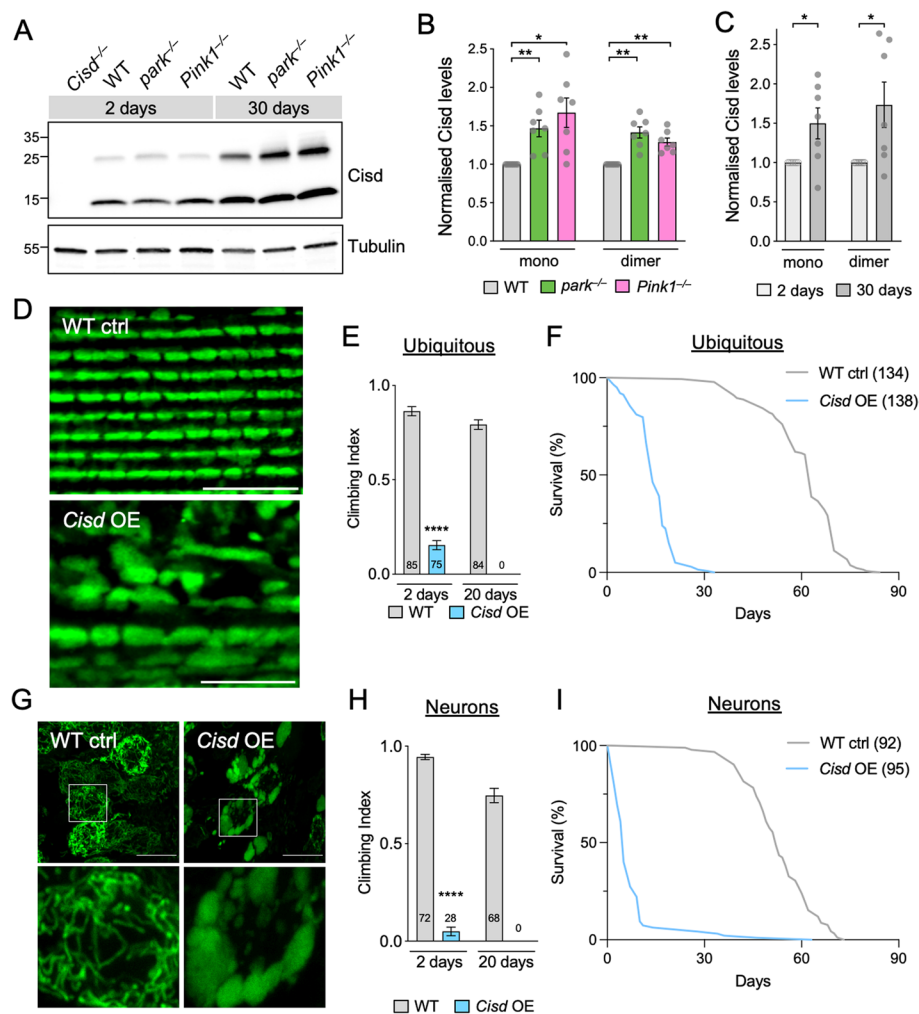
Martinez *et al. Molecular Neurodegeneration* (2024) 19:12

Page 8 of 21

Fig. 1 Cisd accumulation disrupts mitochondria affecting locomotion and lifespan. **A** Representative immunoblot of whole fly lysates of the indicated genotypes from 2- and 30-day-old flies probed for Cisd (CISD2, Proteintech, 13318-1-AP) and Tubulin as loading control. **B**, **C** Quantification of Cisd monomer or dimer levels in 2- and 30-day-old flies analysed in A. **D** Confocal microscopy of flight muscle from 2-day-old wild-type control (WT ctrl) or *Cisd* overexpressing (OE) flies driven by *da*-GAL4, immunostained for ATP5A mitochondrial marker. **E** Climbing assay of 2- and 20-day-old WT and ubiquitous *Cisd* OE flies via the *da*-GAL4 driver. **F** Lifespan of WT and ubiquitous Cisd OE flies. $N > 130$ animals. **G** Confocal microscopy of neuronal soma from control (WT ctrl) or *Cisd* overexpressing (OE) larvae co-expressing the mito-GFP mitochondrial marker via the *nSyb*-GAL4 driver. **H** Climbing assay of 2- and 20-day-old WT and neuronal *Cisd* OE flies via the *nSyb*-GAL4 driver. **I** Lifespan of WT and neuronal *Cisd* OE flies. $N > 90$ animals. Statistical analyses: **B** RM one-way ANOVA with Geisser-Greenhouse correction; **C** paired t-test; **E**, **H** Mann-Whitney non-parametric test. *$P < 0.05$; **$P < 0.01$; ****$P < 0.0001$. Scale bars = 10 μm

samples, as recommended in Prism. When only two groups were compared a Welch's *t* test or Mann-Whitney test was used. All the samples were collected and processed simultaneously and therefore no randomization was appropriate. Unless otherwise indicated, image analysis was done in blind conditions. Statistical analyses were performed using GraphPad Prism 9 software (GraphPad Prism, RRID:SCR_002798). Statistical significance was represented in all cases as follows: *$P < 0.05$, **$P < 0.01$, ***$P < 0.001$ and ****$P < 0.0001$.

Results

Drosophila Cisd accumulates with age, disrupts mitochondria and is neurotoxic

Since Cisd and its homologues have been identified as parkin substrates, we hypothesised that Cisd abundance could be increased in *Drosophila parkin* mutants. Examining the steady-state levels of Cisd, a ~ 14 kDa protein, by immunoblotting we found Cisd levels were increased in aged *parkin* null ($park^{-/-}$) and *Pink1* null mutants ($Pink1^{-/-}$) (Fig. 1A, B). Mammalian CISD1 and CISD2 have been shown to form homodimers with high

Martinez *et al. Molecular Neurodegeneration*   (2024) 19:12

Page 9 of 21

stringency [16, 44]. We also observed Cisd dimers in our immunoblots even under standard reducing conditions (Fig. 1A). In non-reducing conditions, Cisd is almost exclusively found as a dimer (Fig. S1A). We confirmed that the upper band was indeed a dimerised form of Cisd and not a ubiquitinated form as mitochondrial fractions treated with the promiscuous deubiquitinase USP2 retain the dimer band (Fig. S1B). We also noted that Cisd levels increased with age in wild-type (WT) flies (Fig. 1A, C), as previously described [32], with both monomer and particularly the dimer increasing in abundance (Fig. S1A). Age-dependent increase in Cisd was particularly notable in fly head lysates (Fig. S1C, D).

As Cisd levels increased with age, and the Pink1-parkin pathway acts to restrict its steady-state levels, we reasoned that elevated Cisd levels may be a key contributor to age-related organismal decline. Thus, we induced transgenic overexpression of *Cisd* (Fig. S1E), with different tissue-specific drivers, and assessed mitochondrial integrity and organismal fitness and survival. *Cisd* overexpression via the moderate, ubiquitous driver *da*-GAL4 caused gross disruption to mitochondrial morphology, resulting in abnormally enlarged mitochondria in flight muscles (Fig. 1D), as previously reported [32]. It also severely impacted locomotor function and lifespan (Fig. 1E, F). Pan-neuronal overexpression of *Cisd* via *nSyb*-GAL4 also severely affected mitochondrial morphology and locomotion, and dramatically shortened lifespan (Fig. 1G–I). Notably, overexpression restricted just to DA expressing cells via *TH*-GAL4 also caused an age-related decline in motor ability (Fig. S1F), likely reflecting that DA neurons represent only part of a modulatory circuit for reactive locomotion [45], while muscle directed overexpression only caused a modest impact on locomotion and did not significantly affect lifespan (Fig. S1G, H).

Together, these data indicate that Cisd levels accumulate with normal ageing, as well as in *Pink1* and *parkin* mutants, and that Cisd accumulation (especially neuronal accumulation) is sufficient to substantially impact organismal vitality.

Drosophila Cisd is functionally more related to mitochondria-localised CISD1

Both CISD1 and CISD2 have been reported as substrates of Parkin in proteomic studies [14–16]. Evaluating the dynamics of their degradation during PINK1/Parkin-mediated mitophagy, we treated retinal pigment epithelial (RPE1) cells (with endogenous Parkin) or cells overexpressing YFP-Parkin (RPE1-Parkin OE) with antimycin A and oligomycin to induce mitophagy and assessed CISD1 and 2 levels over time (Fig. 2A). Monitoring PINK1-mediated phospho-ubiquitin (pUb) showed rapid induction of

mitophagy that steadily increased over time with a concomitant gradual decrease in the OMM protein TOM20 (Fig. 2A). As expected, pUb deposition, its subsequent turnover, and TOM20 loss was accelerated in Parkin-overexpressing cells. In these conditions, CISD1 was rapidly degraded during mitophagy similar to TOM20, however, we found that CISD2 levels were minimally affected (Fig. 2A). Co-localisation studies analysing the distribution of FLAG-tagged CISD1 or 2 (Fig. 2B) showed that while the majority of CISD1 is localised to mitochondria (TOM20 staining), CISD2 is predominantly localised to the ER (Calnexin staining). These observations are consistent with other reports [22, 24] and align with the degradation of mitochondrial CISD1 while ER-localised CISD2 is largely spared during induced mitophagy.

Drosophila encode a single CISD orthologue with substantial amino acid sequence homology to human CISD1 and CISD2, with marginally higher homology to CISD2 than CISD1 (CISD2; 45% identity, 66% similarity vs. CISD1; 42% identity, 65% similarity). Thus, we sought to determine whether *Drosophila* Cisd may function more similarly to one or other of the human orthologues. Ectopically expressing HA-tagged human *CISD1* and *CISD2* in *Drosophila* neurons, we found that expression of *CISD1* induced the same mitochondrial hyperfused phenotype (Fig. 2C) as seen with overexpression of *Cisd* (Fig. 1G), while *CISD2* expression had minimal effect (Fig. 2C). We previously noted that overexpression of *Drosophila Cisd* triggers mitochondrial pUb accumulation (discussed further below); this was mirrored by expression of *CISD1* but not *CISD2* (Fig. 2D). These results strongly support that *Drosophila* Cisd is functionally more related to CISD1 than CISD2.

Cisd overexpression prevents mitophagy and causes autophagosome accumulation

We recently described that Pink1-mediated pUb can be readily detected in *Drosophila* by immunoblotting or immunohistochemistry [43], and noted that pUb accumulates on dysfunctional mitochondria in *parkin* mutants due to blocked autophagic flux (Fig. 3A, B). Here, we found that *Cisd* overexpression is also sufficient to cause a similar accumulation of pUb by immunoblotting (Fig. 3A). Immunohistochemistry showed a concomitant accumulation of pUb surrounding selected mitochondria in flight muscle (Fig. 3B). The build-up of pUb is consistent with Cisd accumulation blocking efficient mitochondrial degradation and mirrors blocked mitophagy due to the loss of parkin. To verify these observations using an orthogonal approach we analysed mitophagy flux using the *mito-*QC mitophagy reporter flies [8]. This revealed that *Cisd* overexpression caused a significant reduction
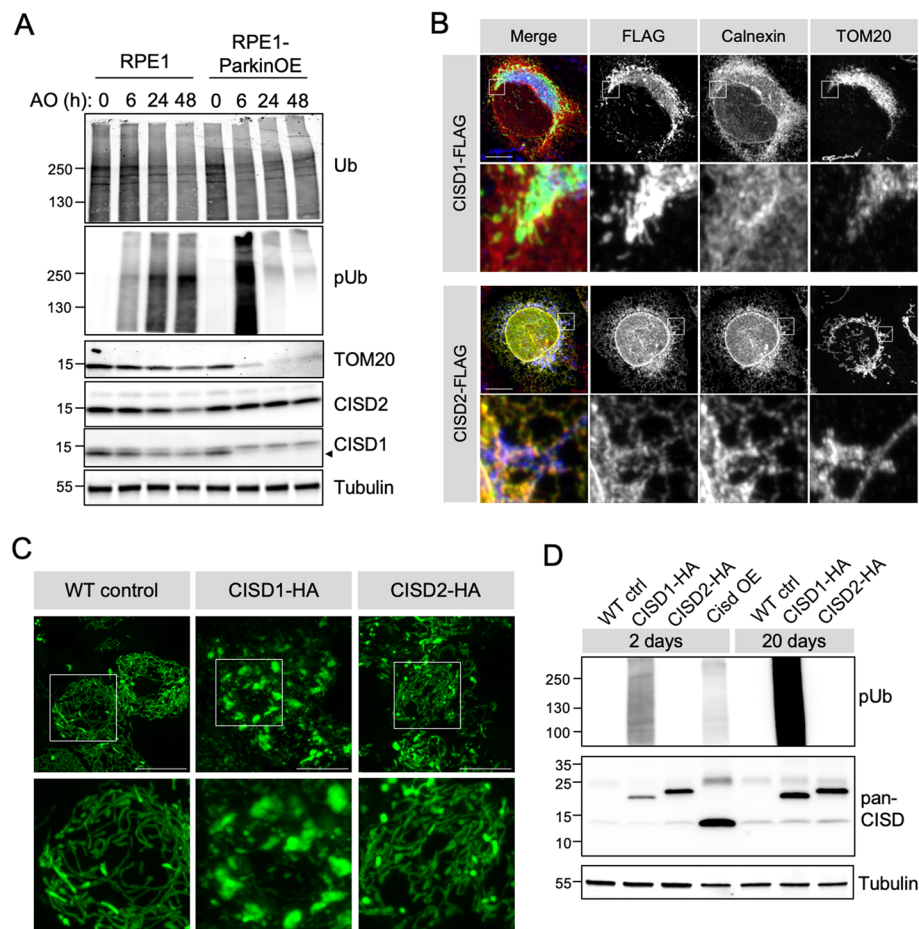
Martinez *et al. Molecular Neurodegeneration* (2024) 19:12

Page 10 of 21

Fig. 2 *Drosophila* Cisd is functionally more similar to CISD1. **A** Immunoblots of protein lysates from RPE1 cells ± YFP-Parkin overexpression (OE) treated with antimycin A (4 μM) and oligomycin (10 μM) for the indicated time to induce mitophagy, probed for mitophagy marker pUb, and degradation of TOM20 and CISD1/2 (CISD1, Proteintech, 16006-1-AP; and CISD2, Proteintech, 13318-1-AP), alongside respective loading control total Ub and Tubulin. Blot is representative of 3 replicate experiments. **B** Confocal micrographs of U2OS cells transfected with human CISD1-FLAG or CISD2-FLAG, counter-stained with antibodies against TOM20 (mitochondria) or Calnexin (ER). **C** Confocal micrographs of *Drosophila* larval neurons expressing transgenic mito-GFP and WT control, human CISD1-HA or CISD2-HA driven by *nSyb*-GAL4. **D** Immunoblots of protein lysates of 2- and 20-day-old whole flies expressing the indicated transgenes via *da*-GAL4 versus WT control, probed for pUb and CISD1/2 with (CISD2, Proteintech, 13318-1-AP). Scale bars = 10 μm

in mitolysosome number in larval and adult neurons (Fig. 3C–F). Thus, *Cisd* overexpression is sufficient to block mitophagy flux.

We postulated that the mitophagy block caused by Cisd accumulation may be due to defective autophagy. To investigate this, we immunostained adult flight muscle overexpressing *Cisd* for the autophagy receptor p62 (also called ref(2)P in *Drosophila*) alongside the autophagosome reporter, mCherry-Atg8a (*Drosophila* homologue of LC3). This showed that p62- and Atg8a-positive puncta accumulate close to mitochondria, forming large aggregates (Fig. 4A). Analysing these structures by electron microscopy confirmed that

indeed numerous autophagosomes accumulate around abnormally enlarged and vesiculated mitochondria in *Cisd* overexpressing tissue (Fig. 4B).

Immunostaining larval brains also revealed an accumulation of p62 puncta upon *Cisd* overexpression, similar to that seen in autophagy-deficient *Atg5* RNAi flies (Fig. 4C). Likewise, immunoblot analysis of *Cisd* overexpressing flies showed increased levels of p62 and accumulation of the lipidated form of *Drosophila* LC3 (Atg8a-II) (Fig. 4D and Fig. S2A, B), indicative of blockage in autophagy flux. Consistent with these observations, the autophagy flux reporter, GFP-mCherry-Atg8a, also showed that autolysosome
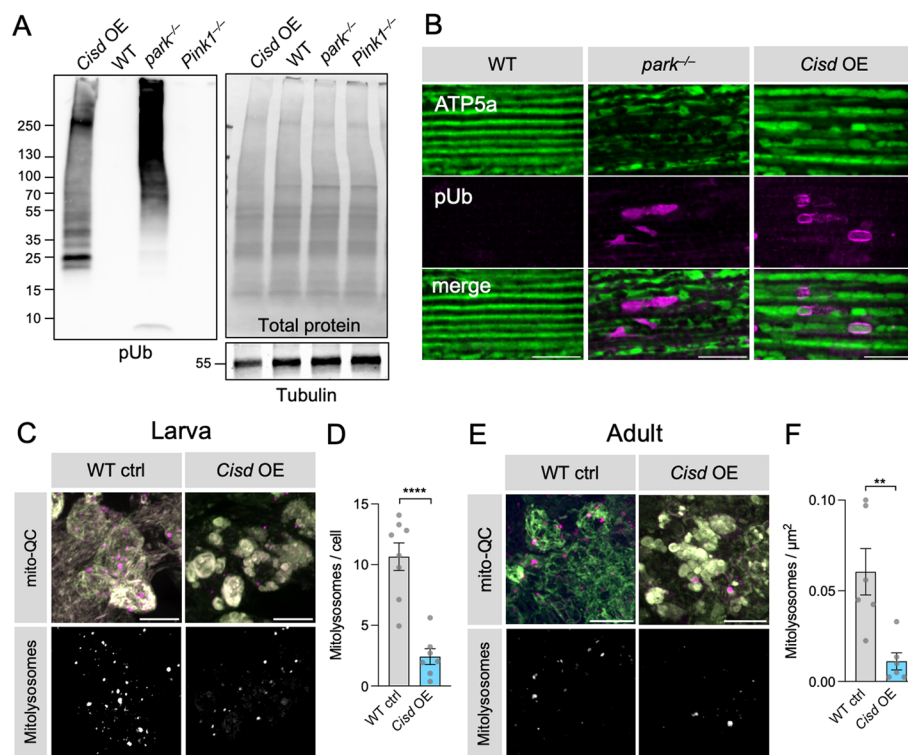
Martinez *et al. Molecular Neurodegeneration* (2024) 19:12

Page 11 of 21

Fig. 3 *Cisd* overexpression blocks mitophagy flux. **A** Immunoblot analysis of whole fly lysates from 2-day-old flies of the indicated genotypes, analysed for pUb, and Tubulin or total protein levels as loading controls. Blot is representative of 3 replicate experiments. *Cisd* overexpression was driven by *da*-GAL4. **B** Confocal microscopy analysis of adult *Drosophila* flight muscle from 2-day-old flies of WT control, *parkin* mutant and *Cisd* overexpression driven by *da*-GAL4 immunostained for mitochondria (ATP5A) and pUb. **C–F** Confocal analysis of mitophagy reporter *mito*-QC (OMM-localised tandem RFP-GFP) of WT or *Cisd* overexpression driven by *nSyb*-GAL4, in larval (**C**, **D**) or adult (**E**, **F**) neurons with 'red-only' mitolysosomes shown. **D**, **F** Number of mitolysosomes quantified shown in C and E. Data points indicate individual animals analysed. Statistical analysis: unpaired t-test; ****P* < 0.01; ******P* < 0.0001. Scale bars = 10 μm

number was significantly decreased in *Cisd* overexpressing muscle (Fig. 4E, F). These data all indicate that maturation of autophagosomes to autolysosomes is impaired.

Finally, complementing these observations with organism-scale genetic manipulations, we found that overexpression of *p62* or *Atg8a* was sufficient to significantly rescue the climbing deficit caused by *Cisd* overexpression (Fig. 4G, H). Interestingly, immunoblot analysis of these animals revealed that upregulation of either p62 or Atg8a significantly reduced the levels of overexpressed Cisd (Fig. 4I and Fig. S2C). The reasons for this are currently unclear and are likely due to increased autophagic flux [33], but certainly correlate well with the phenotypic rescue.

Taken together, these data suggest that the Cisd-related block in mitophagy is caused by an impairment in autophagosome engulfment of defective mitochondria, which ultimately results in autophagosome accumulation and a blockage of general autophagy flux.

Reducing Cisd levels promotes mitophagy in an age- and context-dependent manner

Since Cisd accumulation blocks mitophagy, we reasoned that reducing Cisd levels could have the opposite effect and facilitate mitophagy. To approach this, we first assessed available loss-of-function reagents for *Cisd*. A null mutant, *Cisd*^{−/−}, had significant impact on organismal and mitochondrial phenotypes, conferring shorter lifespan, reduced climbing ability and fragmented mitochondria (Fig. S3A–D), consistent with a previous report [32]. Two independent transgenic *Cisd* RNAi constructs (termed GD and KK), which substantially reduced the Cisd protein levels by 99% and 96%, respectively (Fig. S3A), produced similar but generally milder phenotypes (Fig. S3B–D). Hence, for reasons of greater versatility (i.e., tissue-specific targeting) the RNAi lines were used for subsequent studies and the KK line was preferentially used.

Analysing mitophagic flux using the *mito*-QC reporter, we observed a significant increase in mitophagy with age both in muscle (Fig. 5A, B) and neurons (Fig. S3E, F).
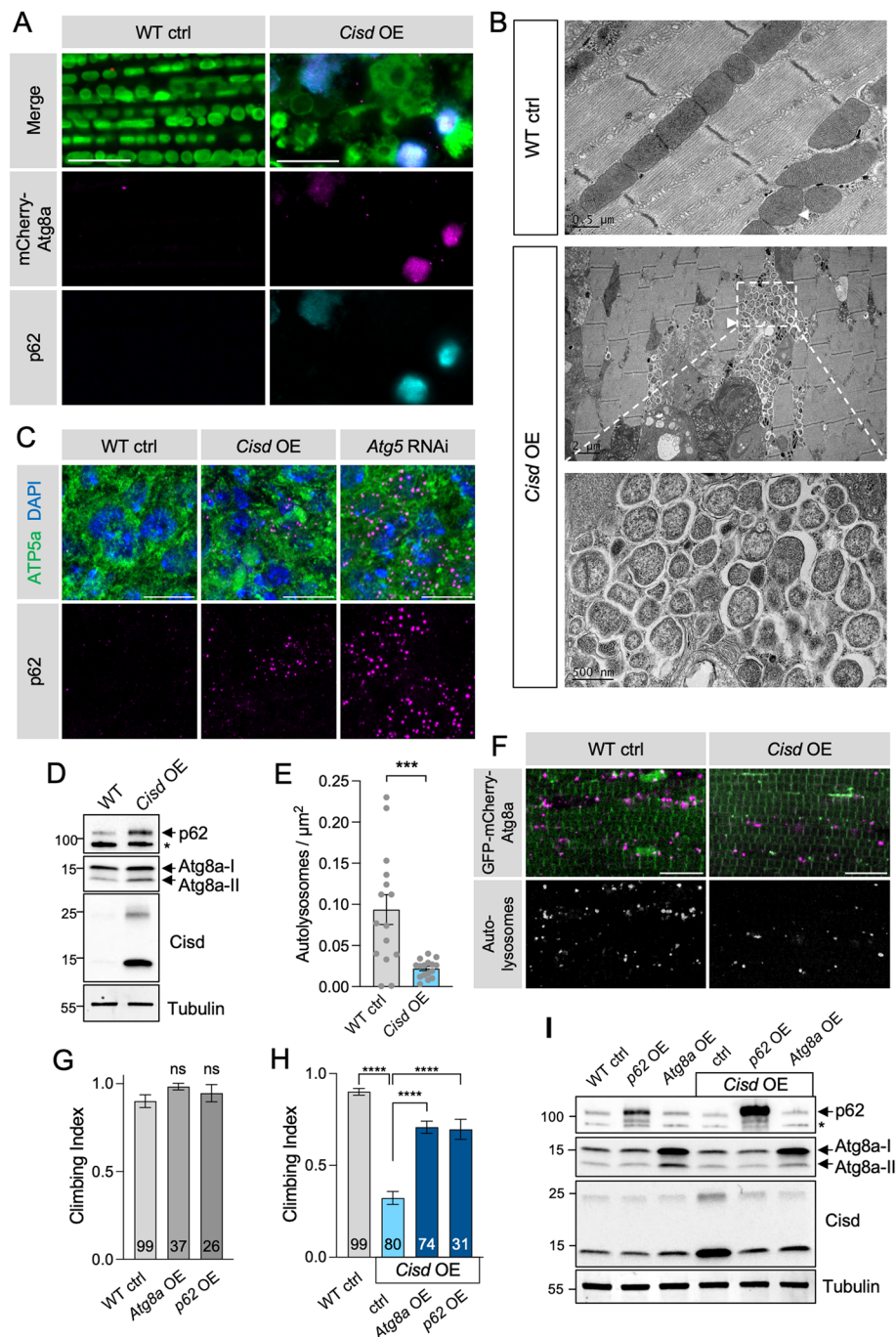
Fig. 4 *Cisd* overexpression causes autophagosome accumulation and prevents autophagy. **A** Confocal micrographs of WT control versus *Cisd* overexpressing adult flight muscle via *Mef2*-GAL4, immunostained for p62 alongside imaging mCherry-Atg8a autophagosome reporter. **B** Electron micrographs of flight muscle as in A, showing multiple autophagic vesicles (inset) in proximity to disrupted mitochondria (arrowheads). **C** Larval neurons of WT control versus *Cisd* overexpressing or *Atg5* knockdown (via *nSyb*-GAL4 driver) animals immunostained for p62 alongside ATP5a (mitochondria) and DAPI. **D** Immunoblot analysis of protein lysates from whole flies overexpressing *Cisd* (via *da*-GAL4) or WT controls. Blots were probed with antibodies against p62, Atg8a (LC3), Cisd (CISD2, Proteintech, 13318-1-AP) and Tubulin. Quantification of replicate blots is shown in Fig. S2A, B. **E** Quantification of the number of autolysosomes shown in F. Data points indicate individual animals analysed. Statistical analysis: unpaired t-test; ***$P < 0.001$. **F** Confocal microscopy analysis of adult flight muscle WT control versus *Cisd* overexpressing animals co-expressing the autophagy flux reporter GFP-mCherry-Atg8a driven by *Mef2*-GAL4. **G, H** Locomotor climbing assay of 2-day-old adult flies expressing the indicated transgenes (via *da*-GAL4). **I** Immunoblot analysis of equivalent samples analysed in G and H, probed for autophagy markers (p62 and Atg8a), Cisd and Tubulin. Quantification of replicate blots is shown in Fig. S2C. Statistical analyses: Kruskal-Wallis non-parametric test with Dunn's post-hoc correction. ***$P < 0.001$; ****$P < 0.0001$. Scale bars = 10 µm for light microscopy, or indicated on image for EM
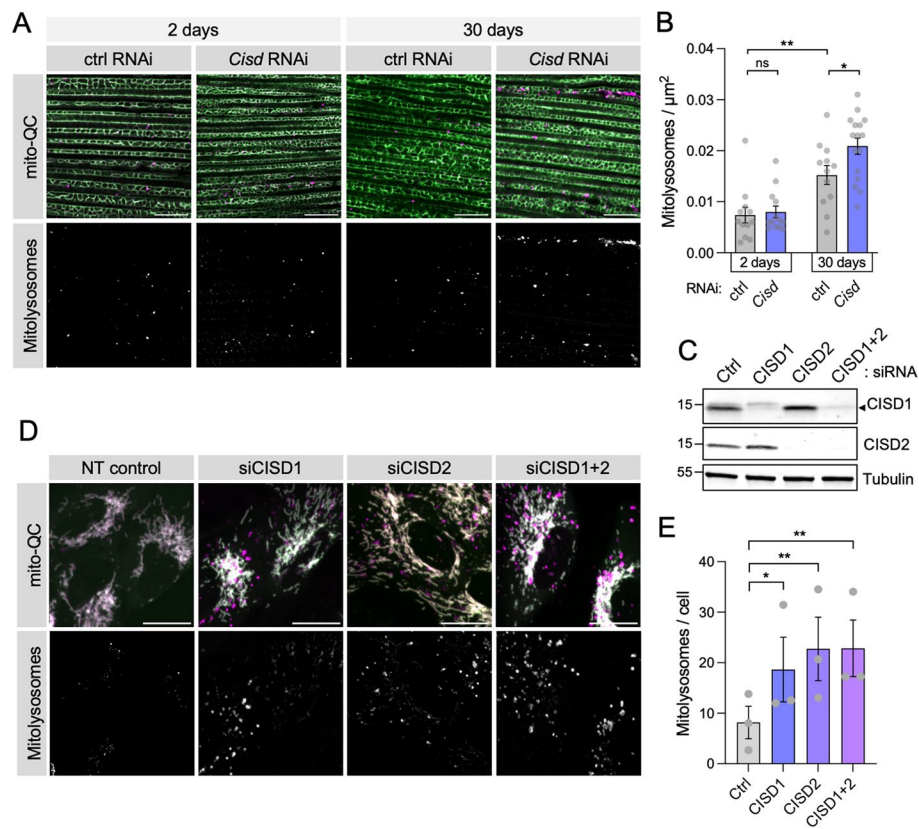
Fig. 5 Loss of *Cisd* promotes mitophagy flux. **A**, **B** Confocal microscopy analysis of mitophagy reporter *mito*-QC in flight muscle from WT control and *Cisd* knockdown flies driven by *Mef2*-GAL4 of the indicated ages. **B** Quantification of the number of mitolysosomes shown in A. Data points indicated individual animals analysed. Statistical analysis: unpaired t-test; *$P < 0.05$; **$P < 0.01$. **C** Immunoblot analysis of ARPE-19 cells expressing *mito*-QC, shown in D, with non-targeting siRNAs (Ctrl) or targeting CISD1, CISD2 or both. **D** Confocal microscopy analysis of mitophagy using *mito*-QC in cells shown in C. **E** Quantification of the number of mitolysosomes shown in D. Data points indicate replicate experiments. Statistical analysis: one-way ANOVA with Dunnett's post-hoc correction; *$P < 0.05$; **$P < 0.01$. Scale bars = 10 μm

Interestingly, *Cisd* knockdown was able to significantly increase mitophagy specifically in muscle tissue of older flies (Fig. 5A, B). No induction was observed in young flies or in aged neurons (Fig. S3E, F). Of note, induction of mitophagy by loss of *Cisd* did not appear to occur via the upregulation of Pink1-mediated pUb as levels were indistinguishable from wild type (Fig. S3G). Moreover, we verified that the effects we observe upon *Cisd* OE/RNAi manipulation were specific to *Cisd* and not due to indirect transcriptional effects on *Pink1* or *parkin* expression (Fig. S2D, E).

Seeking to validate the effect of *Cisd* loss of function in human cells, we knocked down CISD1 and/or CISD2 in a mitophagy reporter cell line (ARPE-19-*mito*-QC) (Fig. 5C) and assessed the formation of mitolysosomes. In agreement with the in vivo data, we found that siRNA-mediated depletion of CISD1, CISD2 or both fragmented mitochondria and significantly increased basal mitophagy (Fig. 5D, E). Together, these data indicate that

reducing CISD levels can increase mitophagy in *Drosophila* and human cells.

Reducing Cisd suppresses *Pink1/parkin* mutant phenotypes by upregulating mitophagy

We have established that Cisd is a key Parkin substrate that accumulates in *Pink1/parkin* mutants and its pathologic build-up induces mitochondrial disruption and neurodegenerative phenotypes. Therefore, we reasoned that reducing Cisd levels in *Pink1/parkin* mutants could ameliorate the pathological phenotypes. *Pink1/parkin* mutants exhibit an array of well characterised neurodegenerative phenotypes, including locomotor deficits, degeneration of flight muscle accompanied by gross mitochondrial disruption, progressive dopaminergic (DA) neuron loss, and shortened lifespan [34, 35, 46]. Ubiquitous knockdown of *Cisd* in *parkin* or *Pink1* mutants significantly suppressed their climbing defects (Fig. 6A, B) and disruption of flight muscle mitochondria
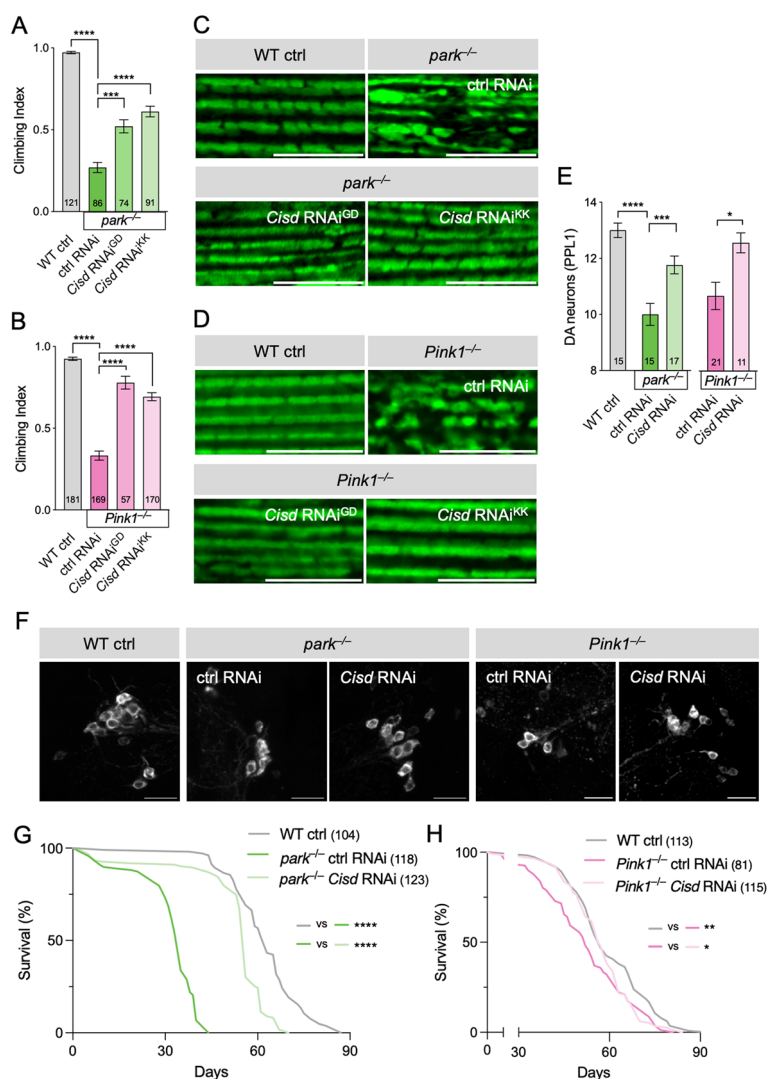
Martinez *et al. Molecular Neurodegeneration* (2024) 19:12

Page 14 of 21

Fig. 6 *Cisd* knockdown ameliorates *Pink1/parkin* mutant phenotypes. **A**, **B** Climbing analysis of WT control versus (**A**) *parkin* or (**B**) *Pink1* mutants with control or *Cisd* RNAi. GD and KK indicate independent RNAi lines driven by *da*-GAL4. See also Fig. S 3B. N is shown inside bars. **C**, **D** Confocal microscopy of flight muscle from (young) wild-type control (WT ctrl) or (**C**) *parkin* or (**D**) *Pink1* mutants expressing control or *Cisd* RNAi stained for the mitochondrial marker ATP5a. **E** Quantification of dopaminergic (DA) neurons shown in F. **F** 30-day-old WT or *parkin* or *Pink1* mutants expressing control or *Cisd* RNAi, immunostained for tyrosine hydroxylase. **G**, **H** Lifespan analysis of WT versus (**G**) *parkin* or (**H**) *Pink1* mutants with control or *Cisd* RNAi. Statistical analyses: (**A**, **B**) Kruskal-Wallis non-parametric test with Dunn's post-hoc correction, (**E**) one-way ANOVA with Sidak's post-hoc correction; (**G**, **H**) Log rank (Mantel-Cox) test. *$P < 0.05$; **$P < 0.01$; ***$P < 0.001$; ****$P < 0.0001$. Scale bars = 10 μm

(Fig. 6C, D). The two RNAi lines suppressed equally well, so for simplicity subsequent experiments were conducted with the KK RNAi line. *Cisd* knockdown also significantly suppressed the degeneration of DA neurons (Fig. 6E, F) and shortened lifespan (Fig. 6G, H) in both *parkin* and *Pink1* mutants. Interestingly, muscle-specific depletion of *Cisd* was sufficient to partially rescue the locomotor phenotype of *parkin* mutants while pan-neuronal knockdown did not (Fig. S4A, B). Overall, these data demonstrate that reduction in Cisd levels is sufficient to significantly reduce the pathology associated

with loss of *Pink1* or *parkin*. Supporting the genetic interaction between *Cisd* and *Pink1/parkin*, it was notable that *Cisd* overexpression, while viable in a wild-type background, caused complete lethality in *Pink1/parkin* mutants (Fig. S4C). Thus, there exists a strong genetic interaction between *Cisd* and *Pink1/parkin* implicating a strong functional interaction.

Having shown that loss of *Cisd* promotes mitophagy in wild-type flies and human cells, we assessed whether reducing Cisd increased mitophagy in the *Pink1/parkin* mutants. As expected, we found that mitochondria

Martinez *et al. Molecular Neurodegeneration* (2024) 19:12

Page 15 of 21

from *Pink1* and *parkin* mutants accumulate high levels of p62 and Atg8a-II (Fig. 7A, B), consistent with a block in mitochondrial turnover, which also occurs upon *Cisd* overexpression (Figs. 4D and 7A and B). In this context, ubiquitous *Cisd* knockdown prevented the aberrant build-up of p62 and Atg8a-II in the *Pink1/parkin* mutants (Fig. 7A, B). Moreover, *Cisd* knockdown also substantially reduced the dramatic build-up of pUb that occurs in *parkin* mutants (Fig. 7C), consistent with a de-repression of the blocked autophagic flux, complementing the p62 analysis. This increased mitophagy flux is not sufficient to fully eliminate pUb build-up, back to WT levels, indicating that additional mechanisms are required. Immunostaining thoraces of these flies showed similar depositions of p62 aggregates in *Pink1* and *parkin* mutants, which were also substantially reduced upon *Cisd* knockdown (Fig. 7D). The reduction in p62 build-up correlated with a notable improvement in mitochondrial morphology in flight muscle, labelled with ATP5a (Fig. 7D). Investigating mitophagy flux directly using the *mito*-QC reporter, we found that, indeed, reducing *Cisd* increased mitophagy in *parkin* or *Pink1* mutant muscle (Fig. 7E–H), which likewise correlated with improved mitochondrial morphology and general tissue health.

Taken together, these data demonstrate that Cisd-depletion induces upregulation of mitophagy independently of Pink1 and parkin, and rescues the abnormal accumulation of pUb, p62 and Atg8a back towards basal levels, preventing neurodegenerative phenotypes in *Pink1* and *parkin* mutant flies. Consistent with these results, the *Cisd* knockdown-induced increase in mitophagy observed in 30-day-old wild-type animals (Fig. 5A, B) was also parkin-independent (Fig. S4D, E). Interestingly, in this experiment mitolysosomes were largely absent in *parkin* mutant muscle, however, this result should be interpreted with caution since it is well documented that flight muscle in *parkin* mutants undergoes apoptosis in young adults [34, 35, 47].

The CISD inhibitor rosiglitazone induces mitophagy and is beneficial for *Pink1/parkin* mutant phenotypes

Given that genetic reduction of *Cisd* levels robustly rescued *Pink1/parkin* phenotypes, we considered the potential for CISD1/2 small-molecule inhibitors to have similar beneficial effects. Several compounds, including rosiglitazone, pioglitazone and NL1, have been reported to potently inhibit CISD1 and CISD2 [48]. Following our findings that CISD1/2 knockdown was sufficient to induce mitophagy, we tested the effects of two structurally distinct compounds, rosiglitazone and NL1, for their potential to induce mitophagy. Exposing mitophagy reporter cells to rosiglitazone and NL1 for 24 h, we found that both compounds intensely induced mitophagy as well as mitochondrial fragmentation (Fig. 8A, B), mirroring the effects of genetically reducing *CISD1/2*.

These results motivated us to test the therapeutic potential of CISD inhibitors in vivo. The preceding results showed that rosiglitazone had an overall greater and more consistent effect on mitophagy induction than NL1, hence, we focussed on rosiglitazone for in vivo analysis. To this end, we treated *Pink1* and *parkin* mutants with rosiglitazone-dosed food and examined their phenotypes. *Pink1/parkin* mutants treated with rosiglitazone showed a modest but significant improvement in their climbing ability (Fig. 8C). There was also a general modest improvement of thoracic indentations and abnormal wing posture (Fig. 8D), caused by the degeneration of underlying flight muscle. Furthermore, rosiglitazone treatment visibly improved mitochondrial morphology of *Pink1/parkin* flight muscle (Fig. 8E). Although dimer levels were modestly reduced, we did not observe major effects on Cisd stability upon rosiglitazone treatment in whole fly lysates (Fig. 8F). Together, these results support the potential benefit of CISD inhibitors in promoting mitophagy and alleviating degenerative phenotypes in these PD models.

Discussion

In this study, we have shown that *Drosophila* Cisd accumulates in *Pink1/parkin* mutant flies, as might be expected from a degradation target, but it also accumulates during normal wild-type ageing. We have demonstrated that *Cisd* overexpression is sufficient to dramatically affect mitochondrial morphology, motor behaviour and lifespan, and is particularly toxic when accumulating in neurons. Considering the conservation with mammalian CISD1/2, our results indicate that *Drosophila* Cisd functions like human CISD1 rather than CISD2, and overexpressing human CISD1 similarly impacts mitochondrial morphology in vivo. Mechanistically, we have found that *Cisd* overexpression blocks mitophagy and inhibits autophagic flux, and in vivo overexpression phenotypes can be suppressed by upregulation of key autophagy regulators. Importantly, we showed that loss of CISD1/Cisd increased mitophagy in human cells and in vivo. Consistent with these effects, genetic loss of *Cisd* significantly rescued *Pink1/parkin* mutant phenotypes, including mitochondrial integrity and DA neurodegeneration. Finally, we demonstrated that known small-molecule CISD inhibitors are able to induce mitophagy in cells and significantly rescue *Pink1/parkin* fly phenotypes, mirroring the genetic reduction. Notably, induction of mitophagy occurs via a Pink1/parkin-independent mechanism. Hence, we posit that CISD1/Cisd proteins play an important role in regulating

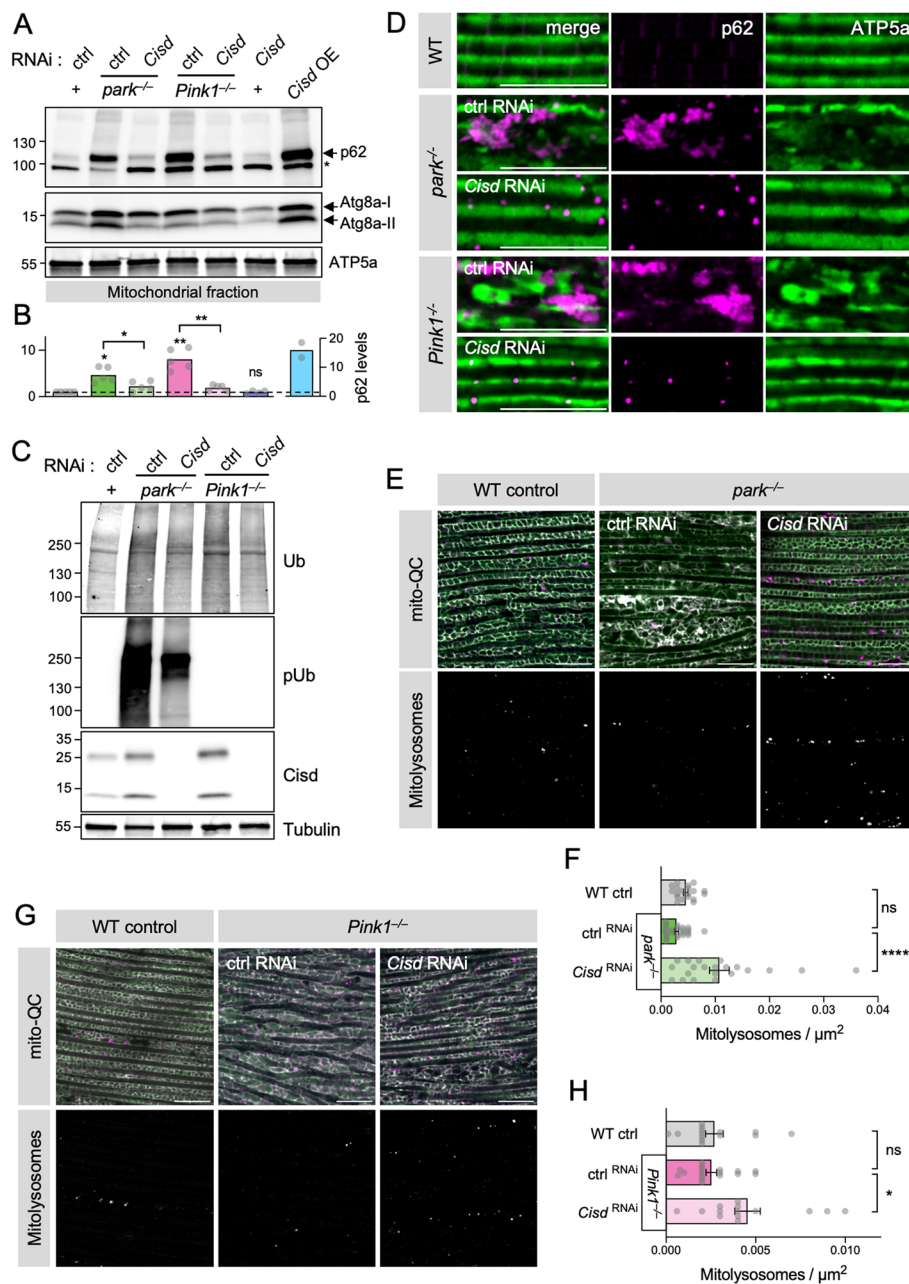Martinez *et al. Molecular Neurodegeneration* (2024) 19:12

Page 16 of 21

Fig. 7 Loss of *Cisd* rescues *Pink1* and *parkin* mutant degenerative phenotypes. **A** Immunoblot of mitochondrial protein lysates from *Cisd* knockdown driven by *da*-GAL4 in WT versus *Pink1* and *parkin* mutant backgrounds, alongside respective controls, probed for p62 and Atg8a (LC3) levels with ATP5a loading control. **B** Relative p62 levels quantified from blots in A, normalised to WT control. Statistical comparisons are against WT control unless indicated. **C** Immunoblots of whole fly lysates of genotypes as in A, probed for pUb, Ub, Cisd (CISD2, Proteintech, 13318-1-AP) and Tubulin as loading control. **D** Confocal micrographs of adult flight muscle from *Cisd* knockdown driven by *da*-GAL4 in WT versus *Pink1* and *parkin* mutant backgrounds, alongside respective controls, immunostained for APT5a and p62. **E** Confocal microscopy analysis of mitophagy reporter *mito*-QC in flight muscle from *Cisd* knockdown driven by *Mef2*-GAL4 in 2-day-old WT and *parkin* mutant backgrounds, alongside WT control. **F** Quantification of the number of mitolysosomes shown in E. **G** Confocal microscopy analysis of mitophagy reporter *mito*-QC in flight muscle from *Cisd* knockdown driven by *Mef2*-GAL4 in 2-day-old WT and *Pink1* mutant backgrounds, alongside WT control. **H** Quantification of the number of mitolysosomes shown in G. Data points indicate individual animals analysed. Statistical analysis: one-way ANOVA with Sidak's post-hoc correction; *$P < 0.05$, **$P < 0.01$; ****$P < 0.0001$. Scale bars = 10 μm
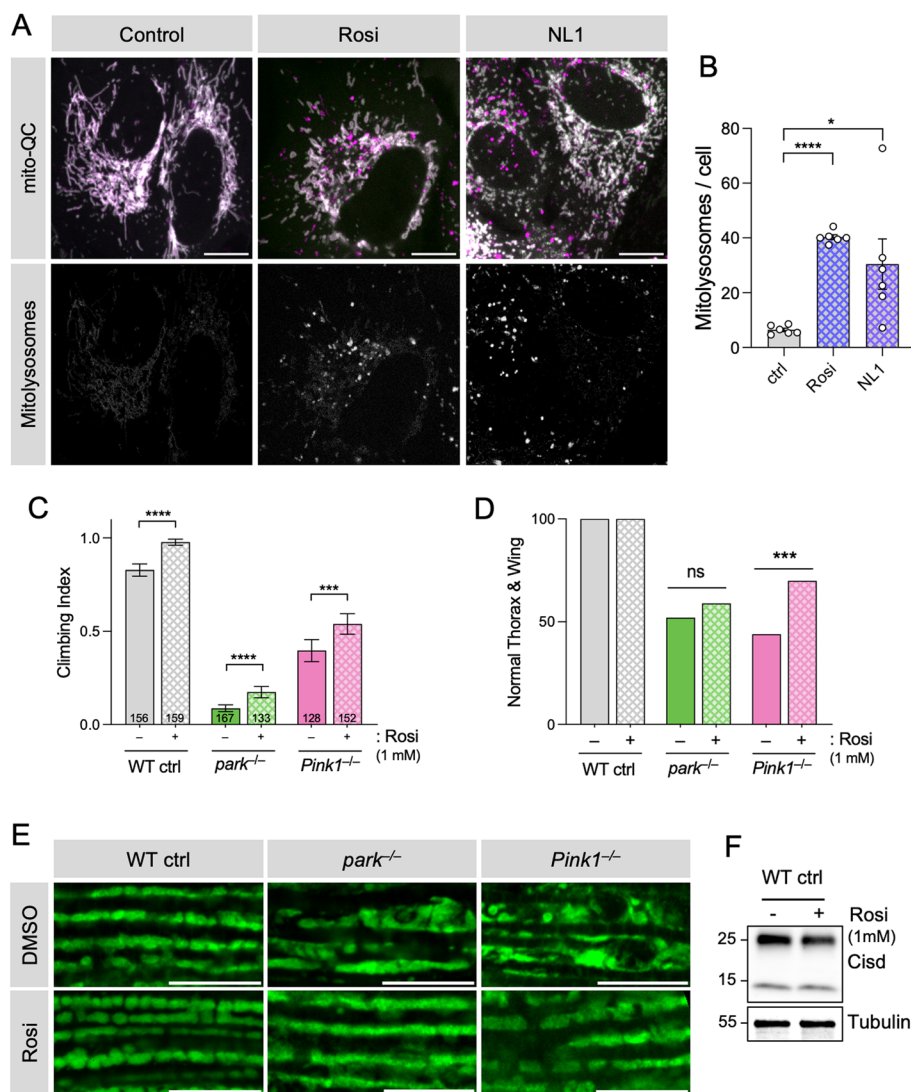
Martinez *et al. Molecular Neurodegeneration* (2024) 19:12

Page 17 of 21

Fig. 8 CISD inhibitors induce mitophagy and rescue rescues *Pink1* and *parkin* mutant phenotypes. **A** Confocal microscopy analysis of WT ARPE-19 cells expressing *mito*-QC to visualise mitolysosomes (shown separately) treated with 100 µM rosiglitazone (Rosi), NL1 or vehicle. **B** Quantification of the number of mitolysosomes per cell of conditions shown in A. Data points indicate replicate experiments. Statistical analysis: RM one-way ANOVA with Geisser-Greenhouse correction; *$P < 0.05$; ****$P < 0.0001$. **C** Analysis of Climbing, (**D**) thoracic indentations and drooped-wing phenotype, and (**E**) mitochondrial morphology in flight muscle of *Pink1* and *parkin* mutants alongside WT control flies, treated with 1 mM rosiglitazone (Rosi) or vehicle. Statistical analysis: Chi-squared test. ***$P < 0.001$; ****$P < 0.0001$. Scale bars = 10 µm. **F** Immunoblot analysis of protein lysates from whole flies upon treatment with 1 mM rosiglitazone (Rosi) or vehicle. Samples were homogenised under reducing conditions and blots were probed for Cisd (CISD2, Proteintech, 13318-1-AP) and Tubulin

mitochondrial function and quality control, ultimately impacting on age-related neurodegeneration.

The [2Fe-2S] cluster-coordinating CISD proteins act as multi-functional regulators of important cellular processes including redox balance, iron metabolism, calcium signalling and mitochondrial respiration [21]. One of the most striking recent developments in understanding the role of CISD proteins is their impact on mitochondrial morphology and dynamics [22, 25, 32, 49–51]. In general, loss of CISD proteins causes mitochondrial fragmentation while their accumulation causes clumping and hyperfusion. Mitochondrial dynamics plays an intimate role in regulating mitochondrial quality control and neuronal survival. Notably, mitochondrial fragmentation is known to facilitate mitophagy [52], consistent with our observations of CISD1/Cisd reduction. Exactly how CISD proteins mediate effects on mitochondrial morphology is not clear; however, CISD1 has been shown to promote

Martinez *et al. Molecular Neurodegeneration* (2024) 19:12

Page 18 of 21

inter-mitochondrial junctions (IMJs) [49], where cristae of neighbouring mitochondria align, likely as a way to couple and enhance respiration [53]. We hypothesise that the enlarged/clumped mitochondrial morphology we observe upon CISD1/Cisd overexpression/accumulation may be a consequence of increased IMJs induced by the strong CISD dimerisation.

Indeed, our finding that Cisd protein levels increased with age, also documented elsewhere [32], suggests further mechanistic links between CISD proteins and age-related mitochondrial disruption. The reason behind the accumulation is unclear at present but could reflect a decline in parkin activity with age or a compensatory response for an increased need for Cisd activity. Since multiple studies have shown that mitochondria become enlarged with age [32, 54–57], and some have linked this to defective autophagy and/or Parkin function [34, 35, 43, 46, 51, 55, 57], it is tempting to speculate that the accumulation of CISD proteins may be a key factor driving mitochondrial clumping/enlargement during ageing. In fact, Chen and colleagues recently showed that age-dependent mitochondrial enlargement is dependent on the progressive increase in Cisd levels [32]. Alternatively, consistent with our data showing that Cisd accumulation inhibits autophagic flux, others report that CISD1/2 may directly regulate autophagy, possibly via modulating Ca^{2+} signalling [29, 31, 51, 57]. Since evidence indicates that proteostasis and autophagy decline with age [58], it is also possible that ageing related decrease in autophagic capacity could also be directly related to increased CISD protein levels.

The abundant evidence that mitochondrial disruption contributes to multiple neurodegenerative diseases [59] and ageing itself [58] has prompted intense interest in identifying ways to upregulate mitophagy as a therapeutic intervention. We have shown that depletion of CISD proteins increased mitophagy in vivo and in human cells. While a recent report suggested that genetic or pharmacologic inhibition of CISD1 induces PINK1-Parkin-mediated mitophagy [60], it should be noted that PINK/Parkin-dependence was not directly assessed in that study. Moreover, care should be taken interpreting data when mitophagy is artificially stimulated by mitochondrial toxins in cellular models since these results might not be physiologically relevant. In contrast, our in vivo data indicate that *Cisd* depletion-induced mitophagy can be PINK1-Parkin-independent since it occurred in *Pink1* and *parkin* mutant flies and did not lead to the induction of PINK1-mediated pUb.

Interestingly, while we found that *Cisd* depletion-induced mitophagy alleviated blocked mitochondrial turnover in *Pink1/parkin* mutants, under steady-state conditions mitophagy induction occurred in quite selective circumstances, notably in aged muscle. Surprisingly, *Cisd* depletion did not have a significant effect on neuronal mitophagy. It is becoming clear that mitophagy rates can greatly vary between tissues [8, 9, 11, 61], and the neurons analysed here displayed higher levels of basal mitophagy (even in young individuals) compared to muscle. Indeed, the differing mitophagy induction perfectly correlated with *Cisd* RNAi being able to rescue *parkin* mutant locomotion defects when expressed in muscle but not in neurons. Altogether, these data suggest that *Cisd* depletion-mediated (Pink1/parkin-independent) mitophagy likely occurs in conjunction with additional stress conditions, for example, with ageing or *Pink1/parkin* related pathology. It will be important for future work to unravel the molecular mechanism of how CISD proteins regulate mitophagy and the circumstance in which this can be unleashed for therapeutic benefit.

Importantly, while this study was being revised, two highly complementary articles emerged which describe very similar mechanistic interactions between CISD/Cisd and Pink1/parkin [62, 63]. Both studies showed similar genetic interactions between *Cisd* and *Pink1/parkin* in *Drosophila* as we found, including the phenotypic rescue of *Pink1/parkin* mutants. Ham and colleagues also showed that pharmacological inhibition (via pioglitazone) of Cisd significantly rescued multiple *Pink1/parkin* phenotypes including DA neurodegeneration [62]. Extending the connection to human DA neurons, Bitar et al. showed that CISD1 dimers aberrantly formed in *PINK1* patient iPSC-derived DA neurons [63]. While Bitar et al. linked this to iron-depleted CISD1 and oxidative stress, the data from Ham and colleagues indicates that Cisd can also modulate IP3R-mediated ER calcium release. Although our data suggest that excess Cisd levels pathologically impinges on autophagy/mitophagy, these mechanisms are not necessarily contradictory or mutually exclusive, cytosolic and mitochondrial calcium regulation of autophagy is hotly debated [64, 65]. Nevertheless, these studies both support our findings, with many of the key results replicated, but also show that further work in required to fully understand the intersection of the proposed mechanisms.

Finally, considering the therapeutic potential of impinging on CISD proteins, several small-molecule inhibitors are currently used as anti-diabetic drugs. CISD1 was originally identified as a target of the thiazolidinedione (TZD) drug, pioglitazone [66], and subsequent studies showed that several distinct TZDs target CISD1 and CISD2 [48]. We have shown that pharmacologic inhibition of CISD proteins via anti-diabetic drugs promotes mitophagy in human cells and provided a modest but significant amelioration of *Pink1/parkin* mutant

Martinez *et al. Molecular Neurodegeneration* (2024) 19:12

Page 19 of 21

phenotypes. While additional work is required to fully evaluate the therapeutic potential of these compounds, it is intriguing to note that epidemiological studies have linked diabetes with an increased risk of PD [67], and diabetic patients treated with anti-diabetic drugs have a reduced risk of developing PD [68, 69].

Conclusion

Cisd naturally accumulates in *Drosophila* tissues during ageing and in *Pink1/parkin*-mutant PD models, causing mitochondrial defects that result in mitophagy and autophagy impairment. Genetic or pharmacological inhibition of Cisd activity alleviates age-related neurodegenerative pathology by upregulating mitophagy, a phenomenon which is conserved in human cells. Thus, we propose that inhibiting CISD proteins, for which FDA-approved drugs are already available, represents a potential therapeutic target for the treatment of neurodegenerative diseases, such as PD but also for age-related decline. Future work is needed to better define the molecular mechanism by which mitophagy is upregulated upon CISD1/2 inhibition and to refine the pharmacokinetics and specificity of potential new inhibitors.

Abbreviations
BSA	Bovine Serum Albumin
DA	Dopaminergic
FBS	Fetal Bovine Serum
FA	Formaldehyde
MQC	Mitochondrial quality control
OMM	Outer mitochondrial membrane
PD	Parkinson's Disease
PBS	Phosphate buffered saline
pUb	Ser65-phospho-Ubiquitin
TZD	Thiazolidinedione
WT	Wild-type

Supplementary Information

The online version contains supplementary material available at https://doi.org/10.1186/s13024-024-00701-3.

Additional file 1: Supplementary Figure S1. Characterisation of *Cisd* in ageing and different tissues**.** (A) Immunoblot analysis of protein lysates from young (2 days) or old (30 days) whole flies of the indicated genotypes. Samples were homogenised under non-reducing (top panel) and reducing (bottom panel) conditions. Blots were probed for Cisd (CISD2, Proteintech, 13318-1-AP) and Tubulin. (B) Immunoblot of mitochondrial fractions from WT flies, probed for poly-Ub, Cisd (CISD2, Proteintech, 13318-1-AP) and ATP5a. (C) Immunoblot analysis of protein lysates from 2- and 30-day-old adult heads of the indicated genotypes, probed for pUb, Cisd (CISD2, Proteintech, 13318-1-AP) and Tubulin. (D) Relative amount of Cisd monomer and dimer quantified from replicate blots shown in C. (E) Immunoblot of protein lysates from whole flies of WT or *Cisd* null (−/−) or *Cisd* overexpression (OE) driven by *da*-GAL4, probed for Cisd (CISD2, Proteintech, 13318-1-AP) and Tubulin. (F, G) Climbing assay of 2- and 20-day-old WT flies or*Cisd* overexpression driven only in (F) DA neurons (*TH*-GAL4) or (G) pan-muscle (*Mef2*-GAL4). (H) Lifespan analysis of flies overexpressing *Cisd* in muscles as in G versus a WT control genotype. Statistical analysis: (D) unpaired t-test; (F, G) Kruskal-Wallis non-parametric test with Dunn's post-hoc correction. ** *P* < 0.01, **** *P* < 0.0001. **Supplementary Figure S2.** Quantification of p62, Atg8-II and Cisd protein levels, and *Pink1* and

---

parkin mRNA. (A, B) Quantification of immunoblots shown in Fig. 4D. (C) Quantification of Cisd levels from immunoblots shown in Fig. 4I. (D, E) Quantification of *Pink1* (D) or *parkin* (E) transcript levels upon *Cisd* overexpression (OE) or knockdown (RNAi). Statistical analysis: (A, B, D, E) Welch's *t* test, (C) one-way ANOVA with Sidak's post-hoc correction. * *P* < 0.05, ** *P* < 0.01, **** *P* < 0.0001. **Supplementary Figure S3.** Characterisation of *Cisd* loss-of-function on organismal and mitochondrial phenotypes. (A) Immunoblot analysis of protein lysates from whole flies of the indicated genotypes of *Cisd* loss versus control, probed for Cisd (CISD2, Proteintech, 13318-1-AP) and Tubulin. (B) Climbing assay of 2- and 20-day-old flies of the indicated genotypes. Knockdown is driven by *da*-GAL4. (C) Lifespan analysis of *Cisd* loss as in B. (D) Confocal microscopy analysis of mitochondrial morphology, immunostained for ATP5A mitochondrial marker in flight muscle of the indicated genotypes. Knockdowns are driven by *da*-GAL4. (E) Confocal analysis of adult neurons of the indicated ages, WT control and *Cisd* RNAi (KK line) animals co-expressing the mitophagy reporter *mito*-QC (OMM-localised tandem RFP-GFP) with *nSyb*-GAL4 to highlight mitolysosomes, shown separately and quantified in F. Statistical analysis: (B) Kruskal-Wallis non-parametric test with Dunn's post-hoc correction. (F) one-way ANOVA with Sidak's post-hoc correction. * *P* < 0.05, **** *P* < 0.0001. Scale bars = 10 μm. (G) Immunoblot analysis of protein lysates from whole flies of the indicated genotypes probed for pUb and Total Ub. **Supplementary Figure S4.** Characterisation of *Cisd*and *parkin* genetic interaction. (A, B) Climbing assay of tissue-specific *Cisd* knockdown (KD) in either pan-muscles with *Mef2*-GAL driver (A) or pan-neurons with *nSyb*-GAL driver (B) alongside respective controls. (C) Viability assay for genetic interactions between the indicated combinations revealing synthetic lethality of *Pink1/parkin* mutants and *Cisd*OE with *da*-GAL driver. (D) Confocal microscopy analysis of mitophagy reporter *mito*-QC in flight muscle from *Cisd* knockdown driven by *Mef2*-GAL4 in WT and *parkin* mutant backgrounds in 30-day-old animals. (E) Quantification of the number of mitolysosomes shown in D. Data points indicated individual animals analysed. Statistical analysis: one-way ANOVA with Sidak's post-hoc correction; * *P* < 0.05, **** *P* < 0.0001. Scale bars = 10 μm.

Authors' contributions

AM and AJW conceived the project; AM, ASM and AW designed the experiments; AM, ASM, JTP, MJT, ATF and PLC performed experimental work; CHC provided key advice, input and reagents; AM, ASM and AW analysed data; AM and AJW wrote the manuscript with input of all co-authors; AJW supervised the project. All authors read and approved the final manuscript.

Availability of data and materials

All data needed to evaluate the conclusions in the paper are present in the paper and/or the Supplementary Materials. This study includes no data deposited in external repositories. Additional data related to this paper may be requested from the authors.

Martinez *et al. Molecular Neurodegeneration* (2024) 19:12

Page 20 of 21

Declarations

Ethics approval and consent to participate
Not applicable.

Consent for publication
Not applicable.

Competing interests
The authors declare that they have no competing interests.

Author details
[1]MRC Mitochondrial Biology Unit, University of Cambridge, Cambridge Biomedical Campus, Hills Road, Cambridge CB2 0XY, UK. [2]Department of Biochemistry and Molecular Biology, Faculty of Science and Technology, UPV/EHU, Leioa, Bizkaia, Spain. [3]National Institute of Infectious Diseases and Vaccinology, National Health Research Institutes, Zhunan, Taiwan.

References
1. Poewe W, Seppi K, Tanner CM, Halliday GM, Brundin P, Volkmann J, et al. Parkinson disease. Nat Rev Dis Primer. 2017;3:1–21.
2. Kitada T, Asakawa S, Hattori N, Matsumine H, Yamamura Y, Minoshima S, et al. Mutations in the parkin gene cause autosomal recessive juvenile parkinsonism. Nature. 1998;392:605–8.
3. Valente EM, Abou-Sleiman PM, Caputo V, Muqit MMK, Harvey K, Gispert S, et al. Hereditary early-Onset Parkinson's Disease caused by mutations in PINK1. Science. 2004;304:1158–60.
4. Narendra D, Tanaka A, Suen D-F, Youle RJ. Parkin is recruited selectively to impaired mitochondria and promotes their autophagy. J Cell Biol. 2008;183:795–803.
5. Narendra DP, Jin SM, Tanaka A, Suen D-F, Gautier CA, Shen J, et al. PINK1 is selectively stabilized on impaired Mitochondria to activate Parkin. PLOS Biol. 2010;8: e1000298.
6. Pickles S, Vigié P, Youle RJ. Mitophagy and Quality Control mechanisms in mitochondrial maintenance. Curr Biol. 2018;28:R170-185.
7. Ge P, Dawson VL, Dawson TM. PINK1 and Parkin mitochondrial quality control: a source of regional vulnerability in Parkinson's disease. Mol Neurodegener. 2020;15:20.
8. Lee JJ, Sanchez-Martinez A, Zarate AM, Benincá C, Mayor U, Clague MJ, et al. Basal mitophagy is widespread in Drosophila but minimally affected by loss of Pink1 or parkin. J Cell Biol. 2018;217:1613–22.
9. McWilliams TG, Prescott AR, Montava-Garriga L, Ball G, Singh F, Barini E, et al. Basal mitophagy occurs independently of PINK1 in mouse tissues of high metabolic demand. Cell Metab. 2018;27:439-449e5.
10. Cornelissen T, Vilain S, Vints K, Gounko N, Verstreken P, Vandenberghe W. Deficiency of parkin and PINK1 impairs age-dependent mitophagy in Drosophila. Youle RJ, editor. eLife. 2018;7:e35878.
11. Kim YY, Um J-H, Yoon J-H, Kim H, Lee D-Y, Lee YJ, et al. Assessment of mitophagy in mt-keima Drosophila revealed an essential role of the PINK1-Parkin pathway in mitophagy induction in vivo. FASEB J. 2019;33:9742–51.
12. Sanchez-Martinez A, Martinez A, Whitworth AJ. FBXO7/ntc and USP30 antagonistically set the ubiquitination threshold for basal mitophagy and provide a target for Pink1 phosphorylation in vivo. PLOS Biol. 2023;21: e3002244.
13. Martinez A, Lectez B, Ramirez J, Popp O, Sutherland JD, Urbé S, et al. Quantitative proteomic analysis of parkin substrates in Drosophila neurons. Mol Neurodegener. 2017;12:29.
14. Sarraf SA, Raman M, Guarani-Pereira V, Sowa ME, Huttlin EL, Gygi SP, et al. Landscape of the PARKIN-dependent ubiquitylome in response to mitochondrial depolarization. Nature. 2013;496:372–6.
15. Ordureau A, Paulo JA, Zhang J, An H, Swatek KN, Cannon JR, et al. Global Landscape and Dynamics of Parkin and USP30-Dependent ubiquitylomes in iNeurons during Mitophagic Signaling. Mol Cell. 2020;77:1124-1142e10.
16. Antico O, Ordureau A, Stevens M, Singh F, Nirujogi RS, Gierlinski M, et al. Global ubiquitylation analysis of mitochondria in primary neurons identifies endogenous parkin targets following activation of PINK1. Sci Adv. 2021;7: eabj0722.
17. Cunningham CN, Baughman JM, Phu L, Tea JS, Yu C, Coons M, et al. USP30 and parkin homeostatically regulate atypical ubiquitin chains on mitochondria. Nat Cell Biol. 2015;17:160–9.
18. Phu L, Rose CM, Tea JS, Wall CE, Verschueren E, Cheung TK, et al. Dynamic regulation of mitochondrial import by the Ubiquitin System. Mol Cell. 2020;77:1107-1123e10.
19. Rusilowicz-Jones EV, Jardine J, Kallinos A, Pinto-Fernandez A, Guenther F, Giurrandino M et al. USP30 sets a trigger threshold for PINK1–PARKIN amplification of mitochondrial ubiquitylation. Life Sci Alliance. 2020 ;3. Available from: https://www.life-science-alliance.org/content/3/8/e202000768. Cited 2023 May 5.
20. Bingol B, Tea JS, Phu L, Reichelt M, Bakalarski CE, Song Q, et al. The mitochondrial deubiquitinase USP30 opposes parkin-mediated mitophagy. Nature. 2014;510:370–5.
21. Nechushtai R, Karmi O, Zuo K, Marjault H-B, Darash-Yahana M, Sohn Y-S, et al. The balancing act of NEET proteins: Iron, ROS, calcium and metabolism. Biochim Biophys Acta BBA - Mol Cell Res. 2020;1867:118805.
22. Bian C, Marchetti A, Hammel P, Cosson P. Intracellular targeting of Cisd2/Miner1 to the endoplasmic reticulum. BMC Mol Cell Biol. 2021;22:48.
23. Lipper CH, Karmi O, Sohn YS, Darash-Yahana M, Lammert H, Song L, et al. Structure of the human monomeric NEET protein MiNT and its role in regulating iron and reactive oxygen species in cancer cells. Proc Natl Acad Sci. 2018;115:272–7.
24. Wiley SE, Murphy AN, Ross SA, van der Geer P, Dixon JE. MitoNEET is an iron-containing outer mitochondrial membrane protein that regulates oxidative capacity. Proc Natl Acad Sci. 2007;104:5318–23.
25. Kusminski CM, Holland WL, Sun K, Park J, Spurgin SB, Lin Y, et al. MitoNEET-driven alterations in adipocyte mitochondrial activity reveal a crucial adaptive process that preserves insulin sensitivity in obesity. Nat Med. 2012;18:1539–49.
26. Landry AP, Wang Y, Cheng Z, Crochet RB, Lee Y-H, Ding H. Flavin nucleotides act as electron shuttles mediating reduction of the [2Fe-2S] clusters in mitochondrial outer membrane protein mitoNEET. Free Radic Biol Med. 2017;102:240–7.
27. Lipper CH, Stofleth JT, Bai F, Sohn Y-S, Roy S, Mittler R, et al. Redox-dependent gating of VDAC by mitoNEET. Proc Natl Acad Sci. 2019;116:19924–9.
28. Amr S, Heisey C, Zhang M, Xia X-J, Shows KH, Ajlouni K, et al. A homozygous mutation in a Novel zinc-finger protein, ERIS, is responsible for Wolfram Syndrome 2. Am J Hum Genet. 2007;81:673–83.
29. Chang NC, Nguyen M, Germain M, Shore GC. Antagonism of beclin 1-dependent autophagy by BCL-2 at the endoplasmic reticulum requires NAF-1. EMBO J. 2010;29:606–18.
30. Wiley SE, Andreyev AY, Divakaruni AS, Karisch R, Perkins G, Wall EA, et al. Wolfram Syndrome protein, Miner1, regulates sulphydryl redox status, the unfolded protein response, and Ca2 + homeostasis. EMBO Mol Med. 2013;5:904–18.
31. Du X, Xiao R, Xiao F, Chen Y, Hua F, Yu S, et al. NAF-1 antagonizes starvation-induced autophagy through AMPK signaling pathway in cardiomyocytes. Cell Biol Int. 2015;39:816–23.
32. Chen P-L, Huang K-T, Cheng C-Y, Li J-C, Chan H-Y, Lin T-Y, et al. Vesicular transport mediates the uptake of cytoplasmic proteins into mitochondria in Drosophila melanogaster. Nat Commun. 2020;11:2592.
33. Aparicio R, Rana A, Walker DW. Upregulation of the Autophagy adaptor p62/SQSTM1 Prolongs Health and Lifespan in Middle-aged Drosophila. Cell Rep. 2019;28:1029-1040e5.
34. Greene JC, Whitworth AJ, Kuo I, Andrews LA, Feany MB, Pallanck LJ. Mitochondrial pathology and apoptotic muscle degeneration in Drosophila parkin mutants. Proc Natl Acad Sci U S A. 2003;100:4078–83.
35. Park J, Lee SB, Lee S, Kim Y, Song S, Kim S, et al. Mitochondrial dysfunction in Drosophila PINK1 mutants is complemented by parkin. Nature. 2006;441:1157–61.
36. Nezis IP, Lamark T, Velentzas AD, Rusten TE, Bjørkøy G, Johansen T, et al. Cell death during Drosophila melanogaster early oogenesis is mediated through autophagy. Autophagy. 2009;5:298–302.
37. Schmittgen TD, Livak KJ. Analyzing real-time PCR data by the comparative CT method. Nat Protoc. 2008;3:1101–8.

Martinez *et al. Molecular Neurodegeneration* (2024) 19:12

Page 21 of 21

38. Terriente-Felix A, Wilson EL, Whitworth AJ. Drosophila phosphatidylinositol-4 kinase fwd promotes mitochondrial fission and can suppress Pink1/parkin phenotypes. Lu B, editor. PLOS Genet. 2020;16:e1008844.

39. Tufi R, Gleeson TP, von Stockum S, Hewitt VL, Lee JJ, Terriente-Felix A, et al. Comprehensive Genetic characterization of mitochondrial Ca2 + Uniporter Components reveals their different physiological requirements in vivo. Cell Rep. 2019;27:1541-1550e5.

40. Ziviani E, Tao RN, Whitworth AJ. Drosophila Parkin requires PINK1 for mitochondrial translocation and ubiquitinates Mitofusin. Proc Natl Acad Sci. 2010;107:5018–23.

41. Whitworth AJ, Theodore DA, Greene JC, Beneš H, Wes PD, Pallanck LJ. Increased glutathione S-transferase activity rescues dopaminergic neuron loss in a Drosophila model of Parkinson's disease. Proc Natl Acad Sci. 2005;102:8024–9.

42. Montava-Garriga L, Singh F, Ball G, Ganley IG. Semi-automated quantitation of mitophagy in cells and tissues. Mech Ageing Dev. 2020;185: 111196.

43. Usher JL, Sanchez-Martinez A, Terriente-Felix A, Chen P-L, Lee JJ, Chen C-H, et al. Parkin drives pS65-Ub turnover independently of canonical autophagy in Drosophila. EMBO Rep. 2022;23:e53552.

44. Paddock ML, Wiley SE, Axelrod HL, Cohen AE, Roy M, Abresch EC, et al. MitoNEET is a uniquely folded 2Fe–2S outer mitochondrial membrane protein stabilized by pioglitazone. Proc Natl Acad Sci. 2007;104:14342–7.

45. Riemensperger T, Isabel G, Coulom H, Neuser K, Seugnet L, Kume K, et al. Behavioral consequences of dopamine deficiency in the *Drosophila* central nervous system. Proc Natl Acad Sci. 2011;108:834–9.

46. Clark IE, Dodson MW, Jiang C, Cao JH, Huh JR, Seol JH, et al. Drosophila pink1 is required for mitochondrial function and interacts genetically with parkin. Nature. 2006;441:1162–6.

47. Ham SJ, Lee D, Yoo H, Jun K, Shin H, Chung J. Decision between mitophagy and apoptosis by Parkin via VDAC1 ubiquitination. Proc Natl Acad Sci. 2020;117:4281–91.

48. Geldenhuys WJ, Skolik R, Konkle ME, Menze MA, Long TE, Robart AR. Binding of thiazolidinediones to the endoplasmic reticulum protein nutrient-deprivation autophagy factor-1. Bioorg Med Chem Lett. 2019;29:901–4.

49. Vernay A, Marchetti A, Sabra A, Jauslin TN, Rosselin M, Scherer PE, et al. MitoNEET-dependent formation of intermitochondrial junctions. Proc Natl Acad Sci U S A. 2017;114:8277–82.

50. Molino D, Pila-Castellanos I, Marjault H-B, Dias Amoedo N, Kopp K, Rochin L, et al. Chemical targeting of NEET proteins reveals their function in mitochondrial morphodynamics. EMBO Rep. 2020;21:e49019.

51. Kusminski CM, Chen S, Ye R, Sun K, Wang QA, Spurgin SB, et al. MitoNEET-Parkin effects in pancreatic α- and β-Cells, Cellular Survival, and Intrainsular Cross Talk. Diabetes. 2016;65:1534–55.

52. Twig G, Shirihai OS. The interplay between mitochondrial dynamics and Mitophagy. Antioxid Redox Signal. 2011;14:1939–51.

53. Picard M, McManus MJ, Csordás G, Várnai P, Dorn IIGW, Williams D, et al. Trans-mitochondrial coordination of cristae at regulated membrane junctions. Nat Commun. 2015;6:6259.

54. Leduc-Gaudet J-P, Picard M, Pelletier FS-J, Sgarioto N, Auger M-J, Vallée J, et al. Mitochondrial morphology is altered in atrophied skeletal muscle of aged mice. Oncotarget. 2015;6:17923–37.

55. Palikaras K, Lionaki E, Tavernarakis N. Coordination of mitophagy and mitochondrial biogenesis during ageing in C. Elegans. Nature. 2015;521:525–8.

56. Brandt T, Mourier A, Tain LS, Partridge L, Larsson N-G, Kühlbrandt W. Changes of mitochondrial ultrastructure and function during ageing in mice and Drosophila. Subramaniam S, editor. eLife. 2017;6:e24662.

57. Liang W, Moyzis AG, Lampert MA, Diao RY, Najor RH, Gustafsson ÅB. Aging is associated with a decline in Atg9b-mediated autophagosome formation and appearance of enlarged mitochondria in the heart. Aging Cell. 2020;19: e13187.

58. López-Otín C, Blasco MA, Partridge L, Serrano M, Kroemer G. Hallmarks of aging: an expanding universe. Cell. 2023;186:243–78.

59. Wang Y, Xu E, Musich PR, Lin F. Mitochondrial dysfunction in neurodegenerative diseases and the potential countermeasure. CNS Neurosci Ther. 2019;25:816–24.

60. Lee S, Lee S, Lee S-J, Chung SW. Inhibition of mitoNEET induces Pink1-Parkin-mediated mitophagy. BMB Rep. 2022;55:354–9.

61. Sun N, Yun J, Liu J, Malide D, Liu C, Rovira II, et al. Measuring in vivo mitophagy. Mol Cell. 2015;60:685–96.

62. Ham SJ, Yoo H, Woo D, Lee DH, Park K-S, Chung J. PINK1 and Parkin regulate IP3R-mediated ER calcium release. Nat Commun. 2023;14:5202.

63. Bitar S, Baumann T, Weber C, Abusaada M, Rojas-Charry L, Ziegler P et al. Mitochondrial CISD1 is a downstream target that mediates PINK1 and Parkin loss-of-function phenotypes. bioRxiv; 2023 . p. 2023.09.28.559909. Available from: https://www.biorxiv.org/content/https://doi.org/10.1101/2023.09.28.559909v1. Cited 2023 Oct 2.

64. Cárdenas C, Foskett JK. Mitochondrial Ca2 + signals in autophagy. Cell Calcium. 2012;52:44–51.

65. Bootman MD, Chehab T, Bultynck G, Parys JB, Rietdorf K. The regulation of autophagy by calcium signals: do we have a consensus? Cell Calcium. 2018;70:32–46.

66. Colca JR, McDonald WG, Waldon DJ, Leone JW, Lull JM, Bannow CA, et al. Identification of a novel mitochondrial protein (mitoNEET) cross-linked specifically by a thiazolidinedione photoprobe. Am J Physiol-Endocrinol Metab. 2004;286:E252-260.

67. Han K, Kim B, Lee SH, Kim MK. A nationwide cohort study on diabetes severity and risk of Parkinson disease. Npj Park Dis. 2023;9:1–8.

68. Brauer R, Wei L, Ma T, Athauda D, Girges C, Vijiaratnam N, et al. Diabetes medications and risk of Parkinson's disease: a cohort study of patients with diabetes. Brain. 2020;143:3067–76.

69. Zhao H, Zhuo L, Sun Y, Shen P, Lin H, Zhan S. Thiazolidinedione use and risk of Parkinson's disease in patients with type 2 diabetes mellitus. NPJ Park Dis. 2022;8:138.

Publisher's Note